Available online at www.sciencedirect.com
ScienceDirect
Comput. Methods Appl. Mech. Engrg. 368 (2020) 113164
Computer methods in applied mechanics and engineering
www.elsevier.com/locate/cma

A stabilized mixed finite element approximation for incompressible finite strain solid dynamics using a total Lagrangian formulation

Inocencio Castañar[a], Joan Baiges[a,*], Ramon Codina[a,b]

[a] Universitat Politècnica de Catalunya, Barcelona Tech, Jordi Girona 1–3, Edifici C1, 08034 Barcelona, Spain
[b] Centre Internacional de Mètodes Numèrics en Enginyeria (CIMNE), Edifici C1, Campus Nord UPC, Gran Capitán S/N, 08034 Barcelona, Spain

Received 27 November 2019; received in revised form 19 May 2020; accepted 20 May 2020
Available online 5 June 2020

Abstract

In this work a new methodology for both the nearly and fully incompressible transient finite strain solid mechanics problem is presented. To this end, the momentum equation is complemented with a constitutive law for the pressure which emerges from the deviatoric/volumetric decomposition of the strain energy function for any hyperelastic material model. The incompressible limit is attained automatically depending on the material bulk modulus. The system is stabilized by means of the Variational Multiscale-Orthogonal Subgrid Scale method based on the decomposition of the unknowns into resolvable and subgrid scales in order to prevent pressure fluctuations. Several numerical examples are presented to assess the robustness and applicability of the proposed formulation.

Keywords: Incompressible hyperelasticity; Solid dynamics; Mixed interpolations; Stabilization methods; Orthogonal subgrid scales

1. Introduction

An incompressible material is understood as the one which keeps its volume constant throughout a motion. In many cases, this is a common idealization and accepted assumption often invoked in continuum and computational mechanics [1]. Numerous polymeric materials can sustain finite strains without noticeable volume changes. Furthermore, many biological materials and several types of soils can be modeled as nearly or fully incompressible [2].

Standard irreducible low order finite elements, in which only the displacement field is considered as the unknown variable of the problem and both stress and strain fields are obtained a posteriori, are typically preferred in complex engineering finite strain solid dynamics problems [3]. Nevertheless, this approach performs poorly in nearly and fully incompressible cases, producing solutions which are completely locked by the constraint. Volumetric and shear locking, pressure fluctuations and poor performance in bending dominated scenarios are some of the effects that can be observed in such situations [4].

Over the last years, different strategies and methodologies have been proposed to reduce or avoid these shortcomings by circumventing the inf–sup conditions (also called Ladyzhenskaya–Babuška–Brezzi (LBB) conditions) [5].

* Corresponding author.
E-mail addresses: icastanar@cimne.upc.edu (I. Castañar), jbaiges@cimne.upc.edu (J. Baiges), ramon.codina@upc.edu (R. Codina).

https://doi.org/10.1016/j.cma.2020.113164
0045-7825/

Reduced and selective integration techniques such as the B-bar, the F-bar or the well-known mean dilatation finite element method avoid these numerical instabilities by reducing the evaluations of the incompressibility constraints at quadrature points. Despite this, these strategies are only prepared to work with structured quadrilateral and structured hexahedral meshes. Many of these displacement-based methods have been shown to be equivalent to mixed methods in which the stresses are approximated by fields of order lower than the displacements over the elements [6].

When considering the static, infinitesimal strain, incompressible case of the solid mechanics problem, we obtain an elliptic problem which is identical to the equations of the Stokes problem in fluid mechanics [7,8]. For this reason, it makes sense to extend the mixed velocity/pressure pair used in the latter to the former for the mixed displacement/pressure approach [9]. This idea facilitated the extension of different implementations in the field of fluid mechanics to the solid mechanics area. See for instance [10–12], a set of works where the incompressible nonlinear material problem is stabilized using the orthogonal subscales method [13,14], a variant of the stabilized method proposed in [15]. These works show the good performance of mixed finite elements using both strains/displacements and stresses/displacements pairs as primary variables. These formulations produce a considerable increase in the number of unknowns per node, but they also increase the accuracy for strains and stresses. Furthermore, in [16] the idea of using displacement/pressure/stress or displacement/pressure/strain formulations was tested and seen to be very effective when solving incompressible cases in which accurate results for stress and strain fields are required.

The majority of the previous works were developed for the static case. When considering the transient case, the elliptic problem becomes hyperbolic due to the second order derivative of the displacements which appears in the momentum equation. To the best of our knowledge, there exist two different effective methodologies in the literature to face this transient problem.

On the one hand, a new first-order mixed form of the equations of finite strain solid dynamics is presented in [17–20]. In these works, the authors propose to use as primary variables the linear momentum $\mathbf{p}$ and the deformation gradient $\mathbf{F}$. In order to effectively solve bending dominated scenarios in nearly incompressible cases they consider the introduction of the jacobian J as an extra unknown [21–23]. In more recent works [24–26], they insert the cofactor tensor of the deformation gradient $\mathbf{H} = \text{cof}\,\mathbf{F}$ as an additional primary variable. The resulting system turns out to be unstable and for this reason, the authors stabilize the problem through a combination of the streamline upwind/Petrov Galerkin (SUPG) stabilization and different penalties on the deformation gradient. This methodology is very promising and it has been tested to be very effective to solve nearly incompressible cases. However, the number of unknowns per node increases drastically taking into account that both $\mathbf{F}$ and $\mathbf{H}$ are non-symmetric tensors.

On the other hand, an effective alternative taking the velocity/pressure pair as unknowns of the problem and updating the displacement explicitly as a final step was proposed in [27,28]. The authors suggest to complement the momentum equation with a rate equation for the evolution of the pressure field and solve it by means of a two-step block Gauss–Seidel strategy, stabilized by means of the Variational Multi-Scale (VMS) method. This formulation is also very powerful despite the necessity of introducing the velocity field as a primary variable of the problem in addition to the pressure field.

In this paper we propose a novel way to solve the solid dynamics problem. Through the well-known deviatoric/volumetric decomposition of the strain energy [29] we complement the momentum equation in the context of the Total Lagrangian framework with the constitutive equation of the pressure. This equation is written so as to allow imposing the incompressibility constraint on hyperelastic materials naturally, introducing any change or additional equation in the system. The complete system which results from this formulation is unstable and it presents the well-known saddle-point structure. The resulting formulation will be stabilized by means of the VMS-Orthogonal SubGrid Scale (OSS) method, which is a stabilization technique well known for its low dissipative and highly accurate performance. The resulting method is very simple and only the addition of a scalar field as an extra primary variable is required.

This work is organized as follows: In Section 2 the solid dynamics equations are summarized as well as the constitutive equation of the additional pressure unknown. Furthermore, the variational form of the problem and the various employed time integrators are introduced. In Section 3 the OSS stabilization technique in hyperelastic models is presented and the stabilized form of the problem is shown. In Section 4 several benchmarks and numerical examples are tested to assess the present formulation and to validate its performance. To end up, in Section 5 some conclusions of the proposed formulation are drawn.

2. Solid dynamics problem

2.1. Conservation equations

In this work, the equations of motion of a body under finite strain assumption are considered. Let Ω and Ω_0 be open, bounded and polyhedral domains of $\mathbb{R}^{\mathrm{d}}$, where $\mathrm{d} \in \{2, 3\}$ is the number of space dimensions. The initial configuration of the body is denoted by Ω_0 whereas the current configuration of the body at time t is denoted by Ω. Any point of the body in the reference configuration is labeled with the reference position vector $\mathbf{X}$. The components of vector $\mathbf{X}$ are considered as the material coordinates. On the other hand, the current position vector $\mathbf{x}$ labels any point of the body at the deformed configuration. We assume the existence of a function ψ which characterizes the motion:

$$\begin{aligned} &\psi : \Omega_0 \longrightarrow \Omega \\ &\mathbf{x} = \psi(\mathbf{X}, t), \quad \forall \mathbf{X} \in \Omega_0, \quad t \geq 0 \end{aligned}$$

The boundary of the reference configuration is denoted as $\Gamma_0 := \partial\Omega_0$ and $\Gamma := \partial\Omega$ represents the boundary of the current configuration. We always assume that the mapping between both boundaries is defined through the motion, $\psi(\Gamma_0) = \Gamma$. We denote as $(0, T)$ the time interval of analysis.

From now on, index notation is also applied identifying a vector or tensor with its Cartesian coordinates either in the reference or the deformed configuration. As usual, repeated indexes imply summation for all space dimensions (see e.g. [1]). To denote scalars, vectors and tensor quantities we use uppercase letters when they are evaluated in the reference configuration and lowercase letters if they are reckoned in the deformed one. We employ the index zero for quantities acting in the reference configuration.

The conservation of linear momentum problem in finite strains for a total Lagrangian formulation framework consists in finding a displacement $\mathbf{u}$ such that

$$\rho_0 \frac{\partial^2 u_a}{\partial t^2} - \frac{\partial}{\partial X_A}\{F_{aB} S_{BA}\} = \rho_0 b_a \quad \text{in } \Omega_0 \times (0, \mathrm{T}) \tag{1}$$

where ρ_0 is the initial density, $\mathbf{F} = \frac{\partial \mathbf{x}}{\partial \mathbf{X}}$ is the deformation gradient, $\mathbf{S}$ is the Second Piola–Kirchhoff (PK2) stress tensor and $\mathbf{b}$ the body forces. Mass conservation implies that

$$\rho J = \rho_0 \tag{2}$$

where $J = \det \mathbf{F}$ is the Jacobian. Let us remark that due to the fact that we are solving the problem in the reference configuration only the initial density is needed. Therefore, there is no need to compute the density at every deformed configuration. With regard to the balance of angular momentum, it implies that the PK2 stress tensor must be symmetric.

In order to be capable of reproducing nearly and fully incompressible scenarios, we introduce the standard decomposition of the Cauchy stress tensor $\boldsymbol{\sigma}$ into its volumetric and deviatoric components:

$$\boldsymbol{\sigma} = \boldsymbol{\sigma}' - p\mathbf{I} \tag{3}$$

where p is the pressure (minus the mean stress) and $\mathbf{I}$ the identity matrix. We can now use the relation between stresses to obtain a proper decomposition for the PK2 stress tensor [30]:

$$S_{AB} = J F^{-1}_{Aa} F^{-1}_{Bb} \sigma_{ab} \overset{(3)}{=} J F^{-1}_{Aa} F^{-1}_{Bb} \sigma'_{ab} - pJ C^{-1}_{AB} := S'_{AB} - pJ C^{-1}_{AB} \tag{4}$$

where we have introduced the deviatoric stresses $\mathbf{S}'$ and the inverse Right Cauchy Tensor $\mathbf{C}^{-1} = \mathbf{F}^{-1}\mathbf{F}^{-T}$. We can now reformulate the conservation of linear momentum (1) by introducing decomposition (4):

$$\rho_0 \frac{\partial^2 u_a}{\partial t^2} - \frac{\partial}{\partial X_A}\left\{F_{aB} S'_{BA}\right\} + \frac{\partial}{\partial X_A}\left\{pJ F^{-1}_{Aa}\right\} = \rho_0 b_a \quad \text{in } \Omega_0 \times (0, \mathrm{T}) \tag{5}$$

Eq. (5) allows us to formulate the linear momentum equation in terms of both displacements $\mathbf{u}$ and pressure p. However, we will need to add an extra equation to obtain a well-posed problem. This equation will be in charge of both providing a constitutive equation for the pressure and imposing the incompressibility constraint. This constitutive equation depends on the type of material considered, and it is presented in the following section.

2.2. Hyperelasticity

In this work we consider isotropic hyperelastic models (see [1,3,30]). These models postulate the existence of a Helmholtz free-energy function (or strain energy function) $\Psi(\mathbf{C})$ such that

$$\mathbf{S} = 2\frac{\partial \Psi(\mathbf{C})}{\partial \mathbf{C}} \tag{6}$$

where $\mathbf{C} = \mathbf{F}^T\mathbf{F}$ is the right Cauchy–Green tensor.

We want to deal with compressible models that can reach the incompressible limit case. To characterize such models, it is convenient to adopt a decoupled representation of the strain energy function of the specific form [1,30]:

$$\Psi(\mathbf{C}) = W\left(\bar{\mathbf{C}}\right) + U(J) \tag{7}$$

where $\bar{\mathbf{C}} = J^{-2/3}\mathbf{C}$ is the volume-preserving part of $\mathbf{C}$. Let us remark that this decomposition allows one to split the elastic response of the material into the so-called deviatoric and volumetric response, respectively. We can now write the PK2 stress tensor by introducing Eq. (7) into Eq. (6):

$$\mathbf{S} = 2\frac{\partial \Psi}{\partial \mathbf{C}} = 2\frac{\partial W}{\partial \mathbf{C}} + 2\frac{\partial U}{\partial \mathbf{C}} = 2\frac{\partial W}{\partial \mathbf{C}} + \frac{dU}{dJ}J\mathbf{C}^{-1} \tag{8}$$

By comparing this equation with Eq. (4) we obtain that:

$$\mathbf{S}' = 2\frac{\partial W}{\partial \mathbf{C}} \quad \text{and} \quad p = -\frac{dU}{dJ} \tag{9}$$

Once we are able to deal with the decoupled form of the strain energy function, we describe a number of constitutive models for both the deviatoric and the volumetric components.

2.2.1. Deviatoric models of the strain energy function

First of all, let us recall that as we are considering isotropic hyperelastic models, the strain energy density must be written in terms of the strain invariants which are defined for the volume-preserving tensor $\bar{\mathbf{C}}$ by

$$\bar{I}_1 = \text{trace } \bar{\mathbf{C}} \tag{10}$$

$$\bar{I}_2 = \frac{1}{2}\left[\left(\text{trace } \bar{\mathbf{C}}\right)^2 - \text{trace}\left(\bar{\mathbf{C}}^2\right)\right] \tag{11}$$

$$\bar{I}_3 = \det \bar{\mathbf{C}} = \det\left(J^{-2/3}\mathbf{C}\right) = 1 \tag{12}$$

From the strains invariants, it can be concluded that $W\left(\bar{\mathbf{C}}\right)$ must be written in terms of the first and second invariants. Let us present suitable functions for the deviatoric component of the strain energy function:

- Neo-Hookean model
  This model results from considering only the first principal invariant

  $$W\left(\bar{I}_1\right) = \frac{\mu}{2}\left(\bar{I}_1 - 3\right) \tag{13}$$

  where μ is the shear modulus. This function involves a single parameter and provides the simplest mathematical model for the nonlinear deformation behavior of rubber-like materials. However, experimental data of several isotropic elastic materials cannot be reproduced by this model and it is worthwhile considering the dependency on $\bar{I}_2$.
- Mooney–Rivlin model
  This model is derived considering the dependance on the second invariant as

  $$W\left(\bar{I}_1, \bar{I}_2\right) = \alpha_1\left(\bar{I}_1 - 3\right) + \alpha_2\left(\bar{I}_2 - 3\right) \tag{14}$$

  where α_1 and α_2 are material parameters that must satisfy $\mu = 2(\alpha_1 + \alpha_2) > 0$. This function is often employed in the description of the behavior of isotropic rubber-like materials. Note that when $\alpha_2 = 0$ we recover the neo-Hookean model.

- Yeoh model
  This model makes the assumption that the variation of the strain energy function with respect to the second invariant is equal to zero and it proposes a three-term function in terms of the first invariant

$$W\left(\bar{I}_1\right) = \alpha_1\left(\bar{I}_1 - 3\right) + \alpha_2\left(\bar{I}_1 - 3\right)^2 + \alpha_3\left(\bar{I}_1 - 3\right)^3 \tag{15}$$

  where α_1, α_2 and α_3 are material parameters which must satisfy that $\mu = 2\alpha_1 + 4\alpha_2\left(\bar{I}_1 - 3\right) + 6\alpha_3\left(\bar{I}_1 - 3\right)^2 > 0$. This model was motivated to simulate the mechanical behavior of carbon-black filled rubber vulcanizates.

Readers are referred to [3,27] for further details on this kind of models.

2.2.2. Volumetric models of the strain energy function

Several nonlinear materials such as rubbers, polymers or soft tissues among others are often slightly compressible and associated with minor dilatational deformations. Due to the decoupled form of the strain energy density, compressibility is accounted for by the volumetric strain energy function. Let us now show some variety of models which are widely used in nonlinear computations and which depend upon the bulk modulus κ.

- Quadratic [31]
  This model is given by the following relation:

$$U(J) = \frac{\kappa}{2}(J-1)^2\,; \quad \frac{dU}{dJ} = \kappa\,(J-1) \tag{16}$$

  Despite of being widely used in practice, this model does not satisfy the fundamental condition of requiring an infinite amount of strain energy in order to compress the body to a single point with vanishing volume state.
- Simo et al. [32]
  This model circumvents the previous problems by adding the logarithm of J as a principal function:

$$U(J) = \frac{\kappa}{4}(\log\,J)^2\,; \quad \frac{dU}{dJ} = \frac{\kappa}{2J}\,\log\,J \tag{17}$$

- Simo–Taylor [32]
  This model satisfies all stability requirements:

$$U(J) = \frac{\kappa}{4}\left(J^2 - 1 - 2\log\,J\right); \quad \frac{dU}{dJ} = \frac{\kappa}{2}\left(J - \frac{1}{J}\right) \tag{18}$$

- Miehe et al. [33]
  In this model, $U(J)$ is given by:

$$U(J) = \kappa\,(J - \log\,J - 1)\,; \quad \frac{dU}{dJ} = \kappa\left(1 - \frac{1}{J}\right) \tag{19}$$

- Liu et al. [34]
  In this model, $U(J)$ is expressed as:

$$U(J) = \kappa\,(J\,\log\,J - J + 1)\,; \quad \frac{dU}{dJ} = \kappa\,\log\,J \tag{20}$$

- Ogden [1]
  For rubber-like materials, Ogden proposed a volumetric response function in terms of the volume ratio J of the following form

$$U(J) = \kappa\frac{1}{\beta^2}\left(\beta\,\log\,J + J^{-\beta} - 1\right); \quad \frac{dU}{dJ} = \frac{\kappa}{\beta J}\left(1 - \frac{1}{J^\beta}\right) \tag{21}$$

  where $\beta > 0$ is an empirical coefficient which must be fixed according to experimental data.

Remark 2.1. It is important to note that all volumetric functions here presented can be written as $U(J) = \kappa G(J)$. Therefore, Eq. (9) can be used to obtain a proper way to impose the incompressibility of a hyperelastic material:

$$p = -\frac{dU}{dJ} \quad \Leftrightarrow \quad p = -\kappa\frac{dG}{dJ} \quad \Leftrightarrow \quad \frac{p}{\kappa} + \frac{dG}{dJ} = 0 \tag{22}$$

This equation can be applied regardless of the compressibility of the material under study. It is interesting to observe that in the incompressible limit, when Poisson's ratio $\nu \to 0.5$ (for isotropic materials) then $\kappa \to \infty$ and Eq. (22) reduces automatically to

$$\frac{dG}{dJ} = 0 \tag{23}$$

For all the volumetric strain energy functions presented here, Eq. (23) imposes directly that $J = 1$ which is in fact the condition that a material must satisfy to be incompressible in finite strains.

2.3. Governing equations

To complete this section, we introduce the mixed solid dynamics problem which consists in finding both a displacement $\mathbf{u}$ and a pressure p such that:

$$\rho_0 \frac{\partial^2 u_a}{\partial t^2} - \frac{\partial}{\partial X_A}\left\{F_{aB} S'_{BA}\right\} + \frac{\partial}{\partial X_A}\left\{p J F^{-1}_{Aa}\right\} = \rho_0 b_a \qquad \text{in } \Omega_0 \times (0, \mathrm{T}) \tag{24}$$

$$\frac{p}{\kappa} + \frac{dG}{dJ} = 0 \qquad \text{in } \Omega_0 \times (0, \mathrm{T}) \tag{25}$$

The governing equations must be supplied with initial conditions of the form $\mathbf{u} = \mathbf{u}^0$, $\frac{\partial \mathbf{u}}{\partial t} = \mathbf{v}^0$ in Ω_0 at $t = 0$, with $\mathbf{u}^0$ and $\mathbf{v}^0$ given, and a set of boundary conditions which can be split into Dirichlet boundary conditions (26), where the displacement is prescribed, or Neumann boundary conditions (27), where the values of tractions $\mathbf{t}_0$ are prescribed:

$$\mathbf{u} = \mathbf{u}_D \quad \text{in } \Gamma_{0,D} \tag{26}$$

$$\mathbf{n}_0\{\mathbf{FS}\} \overset{(4)}{=} \mathbf{n}_0\{\mathbf{FS}'\} - pJ\mathbf{n}_0\mathbf{F}^{-T} = \mathbf{t}_0 \quad \text{in } \Gamma_{0,N} \tag{27}$$

where $\mathbf{n}_0$ is the geometric unit outward normal vector on the boundary of the reference configuration Γ_0.

Remark 2.2. Verifying that this formulation reduces to the mixed formulation in linear elasticity when infinitesimal strains theory is considered is crucial. Regarding the momentum equation (24), the following simplifications are obtained:

$$F_{aB} S'_{BA} \overset{(4)}{\approx} J\sigma'_{ab} \approx \left(1 + \frac{\partial u_c}{\partial x_c}\right)\sigma'_{ab} = \sigma'_{ab} + \cancelto{\approx 0}{(\nabla \cdot \mathbf{u})\sigma'_{ab}} \approx \sigma'_{ab} \tag{28}$$

$$pJ\mathbf{F}^{-1} \approx p\,(1 + \nabla \cdot \mathbf{u})\,\mathbf{I} = p\mathbf{I} + \cancelto{\approx 0}{p\nabla \cdot \mathbf{u}\mathbf{I}} \approx p\mathbf{I} \tag{29}$$

and taking into account that both the reference and current configurations match, we obtain the simplified momentum equation for linear elasticity

$$\rho \frac{\partial^2 u_a}{\partial t^2} - \frac{\partial \sigma'_{ab}}{\partial x_a} + \frac{\partial p}{\partial x_a} = \rho b_a \quad \text{in } \Omega_0 \times (0, \mathrm{T}) \tag{30}$$

With respect to the incompressibility equation (25), as it was previously mentioned, $\frac{dG}{dJ}$ is a function which imposes $J = 1$. Therefore,

$$\frac{p}{\kappa} + \frac{dG}{dJ} \approx \frac{p}{\kappa} + J - 1 \approx \frac{p}{\kappa} + (1 + \nabla \cdot \mathbf{u}) - 1 = \frac{p}{\kappa} + \nabla \cdot \mathbf{u} = 0 \tag{31}$$

which is exactly the constitutive law of the pressure when considering linear elasticity. Let us recall that in the incompressible limit $\kappa \to \infty$, and this equation will reduce automatically to

$$\nabla \cdot \mathbf{u} = 0 \tag{32}$$

which is the incompressibility condition for infinitesimal strain theory.

2.4. Variational form of the problem

We shall use the symbol $\langle \cdot, \cdot \rangle_\omega$ to refer to the integral of the product of two functions, assuming it well-defined. This notation is simplified in the following case: $\langle \cdot, \cdot \rangle_{\Omega_0} \equiv \langle \cdot, \cdot \rangle$.

Let $\mathbb{V}^d$ and $\mathbb{Q}$ be, respectively, the proper functional spaces where displacement and pressure solutions are well-defined for each fixed time $t \in (0, T)$. We denote by $\mathbb{V}_0^d$ functions in $\mathbb{V}^d$ which vanish in the Dirichlet boundary $\Gamma_{0,D}$. We shall be interested also in the spaces $\mathbb{W} := \mathbb{V} \times \mathbb{Q}$, $\mathbb{W}_0 := \mathbb{V}_0 \times \mathbb{Q}$. The variational statement of the problem is derived by testing the system (24)–(25) against arbitrary test functions, $\mathbf{v} \in \mathbb{V}_0^d$ and $q \in \mathbb{Q}$. The weak form of the problem reads: find $\mathbf{U} \equiv [\mathbf{u}, p]^T : (0, T) \to \mathbb{W}$ such that initial conditions are satisfied and

$$\langle \mathbf{V}, \mathfrak{D}_t(\mathbf{U}) \rangle + \mathcal{A}(\mathbf{U}, \mathbf{V}) = \mathcal{F}(\mathbf{V}) \quad \forall \mathbf{V} \in \mathbb{W}_0 \tag{33}$$

where $\mathcal{A}(\mathbf{U}, \mathbf{V})$ is a semilinear form defined on $\mathbb{W} \times \mathbb{W}_0$ as

$$\mathcal{A}(\mathbf{U}, \mathbf{V}) := \left\langle \frac{\partial v_a}{\partial X_A}, F_{aB} S'_{BA} \right\rangle - \left\langle \frac{\partial v_a}{\partial X_A}, pJ F^{-1}_{Aa} \right\rangle + \left\langle q, \frac{dG}{dJ} \right\rangle + \left\langle q, \frac{p}{\kappa} \right\rangle \tag{34}$$

$\mathcal{F}(\mathbf{V})$ is a linear form defined on $\mathbb{W}_0$ as

$$\mathcal{F}(\mathbf{V}) := \langle v_a, \rho_0 b_a \rangle + \langle v_a, t_a \rangle_{\Gamma_{0_N}} \tag{35}$$

and

$$\mathfrak{D}_t(\mathbf{U}) := \left[\rho_0 \frac{\partial^2 \mathbf{u}}{\partial t^2}, 0 \right]^T \tag{36}$$

As usual, integration by parts has been used in order to decrease the continuity requirements of unknowns $\mathbf{u}$ and p and the traction vector $\mathbf{t}_0$ has been identified as $\mathbf{t}_0 = \mathbf{n}_0\{\mathbf{FS}\} \overset{(4)}{=} \mathbf{n}_0\{\mathbf{FS}'\} - pJ\mathbf{n}_0\mathbf{F}^{-T}$.

Let us also remark that the problem can be symmetrized by multiplying (22) by an adequate function that depends on G. In that case the semilinear form $\mathcal{A}(\mathbf{U}, \mathbf{V})$ would derive from a potential.

2.5. Time discretization

In this work implicit time integrators are considered. When the material under study is either nearly or fully incompressible, the Courant–Friedrichs–Lewy (CFL) condition, which involves the bulk modulus, becomes very restrictive. If explicit time integrators are considered, extremely small time steps are needed in order to satisfy it. Furthermore, in the fully incompressible case, as $\kappa \to \infty$, solving the problem with explicit time integration is not possible.

Although in principle any implicit time discretization method can be applied, it has to be taken into account that a hyperbolic system of equations is being solved. It is important to control spurious high-frequency oscillations that might appear in the solution for both nearly and fully incompressible hyperelastic materials. As a consequence, numerical time integrators with high-frequency dissipation will be applied.

Let us now consider a partition of the time interval $[0, T]$ into N time steps of size δt, assumed to be constant.

2.5.1. Backward differentiation formula (BDF)

Given a generic time dependent function at a time step $t^{n+1} = t^n + \delta t$, for $n = 0, 1, 2, \ldots$ the approximation of the time derivative of order $k = 1, 2, \ldots$ is written using information from already computed time instants. In our problem, we have to approximate the second time derivative of the displacement, $\frac{\partial^2 \mathbf{u}}{\partial t^2}^{n+1} := \mathbf{a}^{n+1}$. Depending on the accuracy of the method, we can select specific formulas:

$$\text{BDF1}: \quad \mathbf{a}^{n+1} = \frac{1}{\delta t^2}\{\mathbf{u}^{n+1} - 2\mathbf{u}^n + \mathbf{u}^{n-1}\} + \mathcal{O}(\delta t) \tag{37}$$

$$\text{BDF2}: \quad \mathbf{a}^{n+1} = \frac{1}{\delta t^2}\{2\mathbf{u}^{n+1} - 5\mathbf{u}^n + 4\mathbf{u}^{n-1} - \mathbf{u}^{n-2}\} + \mathcal{O}\left(\delta t^2\right) \tag{38}$$

2.5.2. Newmark-β equations

This is a popular class of time integrators [3]. In this time integration formula, the updated acceleration $\mathbf{a}^{n+1}$ and velocity $\mathbf{v}^{n+1}$ are given by:

$$\begin{aligned}\mathbf{a}^{n+1} &\approx \frac{1}{\beta\delta t^2}\{\mathbf{u}^{n+1}-\mathbf{u}^n-\delta t\mathbf{v}^n-\frac{\delta t^2}{2}(1-2\beta)\,\mathbf{a}^n\}\\ \mathbf{v}^{n+1} &\approx \mathbf{v}^n+(1-\gamma)\,\delta t\mathbf{a}^n+\gamma\delta t\mathbf{a}^{n+1}\end{aligned} \tag{39}$$

Here β and γ are parameters to be tuned. When $\beta = \frac{1}{4}$ and $\gamma = \frac{1}{2}$ the Newmark-β method is implicit, unconditionally stable and at least second-order accurate.

2.6. Linearization

In order to solve the problem, the system needs to be linearized so that a bilinear operator which allows to compute a correction $\boldsymbol{\delta}\mathbf{U}$ of a given guess for the solution at time t^{n+1} is obtained, that we denote by $\mathbf{U}^{n+1}$. Iteration counters will be omitted to simplify the notation. After using a Newton–Raphson scheme, we obtain the following linearized form of the problem. Given $\mathbf{U}^{n+1}$ as the solution at time t^{n+1} and the previous iteration, find a correction $\delta\mathbf{U}\equiv[\delta\mathbf{u},\delta p]^T:(0,T)\to\mathbb{W}_0$ such that

$$\left\langle\mathbf{V},\mathfrak{D}_t\left(\mathbf{U}^{n+1}+\delta\mathbf{U}\right)\right\rangle+\mathcal{B}\left(\delta\mathbf{U},\mathbf{V}\right)=\mathcal{F}\left(\mathbf{V}\right)-\mathcal{A}\left(\mathbf{U}^{n+1},\mathbf{V}\right)\quad\forall\mathbf{V}\in\mathbb{W}_0 \tag{40}$$

where $\mathcal{B}(\delta\mathbf{U},\mathbf{V})$ is the bilinear form obtained through the Newton–Raphson linearization and it is defined on $\mathbb{W}_0\times\mathbb{W}_0$ as

$$\begin{aligned}\mathcal{B}\left(\delta\mathbf{U},\mathbf{V}\right)=&\left\langle\frac{\partial v_a}{\partial X_A},\frac{\partial\delta u_a}{\partial X_B}S'_{BA}\right\rangle+\left\langle\frac{\partial v_a}{\partial X_A},F_{aB}\delta S'_{BA}\right\rangle-\left\langle\frac{\partial v_a}{\partial X_A},JpF^{-1}_{Bb}\frac{\partial\delta u_b}{\partial X_B}F^{-1}_{Aa}\right\rangle\\&+\left\langle\frac{\partial v_a}{\partial X_A},JpF^{-1}_{Ab}\frac{\partial\delta u_b}{\partial X_B}F^{-1}_{Ba}\right\rangle-\left\langle\frac{\partial v_a}{\partial X_A},J\delta pF^{-1}_{Aa}\right\rangle+\left\langle q,\mathrm{f}(J)\,F^{-1}_{Aa}\frac{\partial\delta u_a}{\partial X_A}\right\rangle+\left\langle q,\frac{\delta p}{\kappa}\right\rangle\end{aligned} \tag{41}$$

where $\mathrm{f}(J)$ is a function coming from the linearization of $\frac{dG}{dJ}$ and depends upon the volumetric strain energy function into consideration and $\delta S'_{BA}$ is the first term in the decomposition of the PK2 tensor computed with $\delta\mathbf{u}$. Let us remark that all terms are evaluated at $\mathbf{U}^{n+1}$.

It is quite simple to observe that for every implicit time integrator presented here, we can write:

$$\frac{\partial^2\left(\mathbf{u}^{n+1}+\delta\mathbf{u}\right)}{\partial t^2}=\frac{C_a}{\delta t^2}\delta\mathbf{u}+\mathbf{a}^{n+1} \tag{42}$$

where C_a is a coefficient depending on the scheme and $\mathbf{a}^{n+1}$ is the acceleration computed for a given iteration.

Therefore, we can write the time discretized form of $\mathfrak{D}_t\left(\mathbf{U}^{n+1}+\delta\mathbf{U}\right)$ at time step $t^{n+1}=t^n+\delta t$ as:

$$\mathfrak{D}_t\left(\mathbf{U}^{n+1}+\delta\mathbf{U}\right)\approx\mathfrak{D}_{\delta u}\left(\delta\mathbf{U}\right)+\mathfrak{D}_t\left(\mathbf{U}^{n+1}\right)=\rho_0\left[\frac{C_a}{\delta t^2}\delta\mathbf{u},0\right]^T+\rho_0\left[\mathbf{a}^{n+1},0\right]^T \tag{43}$$

and problem (40) can be written after time discretization as:

$$\left\langle\mathbf{V},\mathfrak{D}_{\delta u}\left(\delta\mathbf{U}\right)\right\rangle+\mathcal{B}\left(\delta\mathbf{U},\mathbf{V}\right)=\mathcal{F}\left(\mathbf{V}\right)-\mathcal{A}\left(\mathbf{U}^{n+1},\mathbf{V}\right)-\left\langle\mathbf{V},\mathfrak{D}_t\left(\mathbf{U}^{n+1}\right)\right\rangle\quad\forall\mathbf{V}\in\mathbb{W}_0 \tag{44}$$

2.7. Galerkin spatial discretization

The standard Galerkin approximation of this abstract variational problem is now straightforward. Let $\mathcal{P}_h$ denote a finite element partition of the domain Ω_0. The diameter of an element domain $K\in\mathcal{P}_h$ is denoted by h_K and the diameter on the finite element partition by $h=\max\{h_K|K\in\mathcal{P}_h\}$. We can now construct conforming finite element spaces $\mathbb{V}_h\subset\mathbb{V}$, $\mathbb{Q}_h\subset\mathbb{Q}$ and $\mathbb{W}_h=\mathbb{V}_h\times\mathbb{Q}_h$ in the usual manner, as well as the corresponding subspaces $\mathbb{V}_{h,0}\subset\mathbb{V}_0$ and $\mathbb{W}_{h,0}=\mathbb{V}_{h,0}\times\mathbb{Q}_h$, $\mathbb{V}_{h,0}$ being made with functions that vanish on the Dirichlet boundary. In principle, functions in $\mathbb{V}_h$ are continuous, whereas functions in $\mathbb{Q}_h$ not necessarily.

The Galerkin discrete version of problem (44) is: For a given time t^{n+1} and a fixed iteration, find $\delta\mathbf{U}_h\in\mathbb{W}_{h,0}$ such that

$$\left\langle\mathbf{V}_h,\mathfrak{D}_{\delta u}\left(\delta\mathbf{U}_h\right)\right\rangle+\mathcal{B}\left(\delta\mathbf{U}_h,\mathbf{V}_h\right)=\mathcal{F}\left(\mathbf{V}_h\right)-\mathcal{A}\left(\mathbf{U}_h^{n+1},\mathbf{V}_h\right)-\left\langle\mathbf{V}_h,\mathfrak{D}_t\left(\mathbf{U}_h^{n+1}\right)\right\rangle\quad\forall\mathbf{V}_h\in\mathbb{W}_{h,0} \tag{45}$$

The well posedness of this problem relies on an inf–sup condition [5]. This condition is necessary and sufficient for the existence and uniqueness of the solution to the discrete saddle-point problem. Convenient displacement–pressure interpolations, such as equal interpolation, turn out to violate the inf–sup condition. This is why the so-called stabilized formulations have been proposed to approximate this kind of problems. The main idea is to replace (44) by another discrete variational problem in which the bilinear form $\mathcal{B}$ is enhanced so that it has improved stability properties. In order to overcome the instabilities previously discussed, we propose the stabilization technique described in the next section.

Remark 2.3. Taking a look on the bilinear form $\mathcal{B}$ one should notice that the only term which involves q and δp is $\frac{1}{\kappa}\langle q, \delta p\rangle$ Hence, in the nearly and fully incompressible cases, when $\kappa \to \infty$, this term vanishes causing the saddle-point structure of the problem to appear.

3. Incompressible solid dynamics stabilized finite element formulation

The stabilized finite element method we propose in the following is based on the VMS concept [15,35]. Let $\mathbb{W} = \mathbb{W}_h \oplus \tilde{\mathbb{W}}$, where $\tilde{\mathbb{W}}$ is any space to complete $\mathbb{W}_h$ in $\mathbb{W}$. $\tilde{\mathbb{W}}$ will be approximated by a finite-dimensional space despite the fact that it is infinite-dimensional. The elements of this space are denoted by $\tilde{\mathbf{U}} \equiv \left[\tilde{\mathbf{u}}, \tilde{p}\right]^T$ and they are called subscales. Likewise, let $\mathbb{W}_0 = \mathbb{W}_{h,0} \oplus \tilde{\mathbb{W}}_0$.

Taking into account that $\mathcal{B}$ is a bilinear form, the continuous problem (44) is equivalent to find $\delta\mathbf{U} \in \mathbb{W}_h$ and $\tilde{\mathbf{U}} \in \tilde{\mathbb{W}}$ such that

$$\begin{aligned}
&\langle \mathbf{V}_h, \mathfrak{D}_{\delta u}(\delta\mathbf{U}_h)\rangle + \left\langle \mathbf{V}_h, \mathfrak{D}_{\delta u}\left(\tilde{\mathbf{U}}\right)\right\rangle + \mathcal{B}\left(\delta\mathbf{U}_h, \mathbf{V}_h\right) + \mathcal{B}\left(\tilde{\mathbf{U}}, \mathbf{V}_h\right) \\
&\quad = \mathcal{F}\left(\mathbf{V}_h\right) - \mathcal{A}\left(\mathbf{U}_h^{n+1}, \mathbf{V}_h\right) - \left\langle \mathbf{V}_h, \mathfrak{D}_t\left(\mathbf{U}_h^{n+1}\right)\right\rangle \quad \forall \mathbf{V}_h \in \mathbb{W}_{h,0} \qquad (46)\\
&\left\langle \tilde{\mathbf{V}}, \mathfrak{D}_{\delta u}(\delta\mathbf{U}_h)\right\rangle + \left\langle \tilde{\mathbf{V}}, \mathfrak{D}_{\delta u}\left(\tilde{\mathbf{U}}\right)\right\rangle + \mathcal{B}\left(\delta\mathbf{U}_h, \tilde{\mathbf{V}}\right) + \mathcal{B}\left(\tilde{\mathbf{U}}, \tilde{\mathbf{V}}\right) \\
&\quad = \mathcal{F}\left(\tilde{\mathbf{V}}\right) - \mathcal{A}\left(\mathbf{U}_h^{n+1}, \tilde{\mathbf{V}}\right) - \left\langle \tilde{\mathbf{V}}, \mathfrak{D}_t\left(\mathbf{U}_h^{n+1}\right)\right\rangle \quad \forall \tilde{\mathbf{V}} \in \tilde{\mathbb{W}} \qquad (47)
\end{aligned}$$

where Eq. (46) is called the finite element scale equation and (47) is called the subgrid scale equation. Note that in Eq. (46), the term $\mathcal{B}\left(\tilde{\mathbf{U}}, \mathbf{V}_h\right)$ is obtained from directly linearizing $\mathcal{A}\left(\tilde{\mathbf{U}}, \mathbf{V}_h\right)$.

The main idea behind any stabilized finite element method derived from the VMS framework is to obtain an expression for the subscales from the subgrid scale equation (47) in order to complement our finite element scale equation (46). First of all let us make some assumptions about the subgrid scale functions. In this work we consider the subscales to be quasi-static, which means that they are not time-dependent:

$$\frac{\partial^2 \tilde{\mathbf{u}}}{\partial t^2} \approx \mathbf{0} \quad \Leftrightarrow \quad \mathfrak{D}_{\delta u}\left(\tilde{\mathbf{U}}\right) \approx [0,0]^T \qquad (48)$$

Remark 3.1. Note that the contribution from the transient evolution of the subscales can be kept. In this case, the subscales are called to be time-dependent or dynamic subscales [13]. The cost it implies is the storage of the subscales in previous time steps.

We also assume the subscale to behave as bubble functions, which means that they vanish across inter-element boundaries. Taking this into account, we can integrate by parts within each element in Eq. (47) to obtain:

$$\begin{aligned}
&\sum_K \left\langle \tilde{\mathbf{V}}, \mathfrak{D}_{\delta u}(\delta\mathbf{U}_h)\right\rangle_K + \sum_K \left\langle \tilde{\mathbf{V}}, \mathfrak{B}(\delta\mathbf{U}_h)\right\rangle_K + \sum_K \left\langle \tilde{\mathbf{V}}, \mathfrak{B}\left(\tilde{\mathbf{U}}\right)\right\rangle_K \\
&\quad = \sum_K \left\langle \tilde{\mathbf{V}}, \mathfrak{F}\right\rangle_K - \sum_K \left\langle \tilde{\mathbf{V}}, \mathfrak{A}\left(\mathbf{U}_h^{n+1}\right)\right\rangle_K - \sum_K \left\langle \tilde{\mathbf{V}}, \mathfrak{D}_t\left(\mathbf{U}_h^{n+1}\right)\right\rangle_K \quad \forall \tilde{\mathbf{V}} \in \tilde{\mathbb{W}} \qquad (49)
\end{aligned}$$

where $\sum_K$ stands for the summation over all $K \in \mathcal{P}_h$ and $\mathfrak{B}(\delta\mathbf{U}_h) = \left[\mathfrak{B}_u(\delta\mathbf{U}_h), \mathfrak{B}_p(\delta\mathbf{U}_h)\right]^T$ is a linear operator coming from the integration by parts of $\mathcal{B}$ such that $\mathcal{B}\left(\delta\mathbf{U}_h, \tilde{\mathbf{V}}\right) = \sum_K \left\langle \tilde{\mathbf{V}}, \mathfrak{B}(\delta\mathbf{U}_h)\right\rangle_K$ and it is defined as:

$$\begin{aligned}
\mathfrak{B}_u(\delta\mathbf{U}_h)_a = &-\frac{\partial}{\partial X_A}\left\{\frac{\partial \delta u_{h,a}}{\partial X_B} S'_{BA}\right\} - \frac{\partial}{\partial X_A}\left\{F_{aB}\delta S'_{BA}\right\} + \frac{\partial}{\partial X_A}\left\{J p_h F^{-1}_{Bb}\frac{\partial \delta u_{h,b}}{\partial X_B}F^{-1}_{Aa}\right\} \\
&- \frac{\partial}{\partial X_A}\left\{J p_h F^{-1}_{Ab}\frac{\partial \delta u_{h,b}}{\partial X_B}F^{-1}_{Ba}\right\} + \frac{\partial}{\partial X_A}\left\{J\delta p_h F^{-1}_{Aa}\right\}
\end{aligned}$$

$$\mathfrak{B}_p\left(\delta\mathbf{U}_h\right) = \mathrm{f}\left(J\right) F^{-1}_{Aa} \frac{\partial \delta u_{h,a}}{\partial X_A}$$

A similar expression is found for $\mathfrak{B}\left(\tilde{\mathbf{U}}\right)$ in (49).

Regarding the right-hand side, $\mathfrak{F} = \left[\mathfrak{F}_u, \mathfrak{F}_p\right]^T$ appears from the external forces form $\mathcal{F}$ and it is given by:

$$\mathfrak{F}_{u.a} = \rho_0 b_a \quad ; \quad \mathfrak{F}_p = 0 \tag{50}$$

and finally $\mathfrak{A}\left(\mathbf{U}_h^{n+1}\right) = \left[\mathfrak{A}_u\left(\mathbf{U}_h^{n+1}\right), \mathfrak{A}_p\left(\mathbf{U}_h^{n+1}\right)\right]^T$ comes from the integration by parts of $\mathcal{A}$ and it is defined as:

$$\begin{aligned} \mathfrak{A}_u\left(\mathbf{U}_h^{n+1}\right)_a &= -\frac{\partial}{\partial X_A}\{F_{aB} S'_{BA}\} + \frac{\partial}{\partial X_A}\{J p_h F^{-1}_{Aa}\} \\ \mathfrak{A}_p\left(\mathbf{U}_h^{n+1}\right) &= \frac{dG}{dJ} \end{aligned} \tag{51}$$

Remark 3.2. In the case of linear elements, for which second order derivatives of finite element functions in the element interiors vanish, these expressions reduce significantly so that it is worthwhile to make them explicit:

$$\begin{aligned} \mathfrak{B}_u\left(\delta\mathbf{U}_h\right)_a &= J\frac{\partial p_h}{\partial X_A} F^{-1}_{Bb} \frac{\partial \delta u_{h,b}}{\partial X_B} F^{-1}_{Aa} - J\frac{\partial p_h}{\partial X_A} F^{-1}_{Ab} \frac{\partial \delta u_{h,b}}{\partial X_B} F^{-1}_{Ba} + J\frac{\partial \delta p_h}{\partial X_A} F^{-1}_{Aa} \\ \mathfrak{A}_u\left(\mathbf{U}_h^{n+1}\right) &= J\frac{\partial p_h}{\partial X_A} F^{-1}_{Aa} \end{aligned}$$

Eq. (49) must be satisfied for all elements $K \in \mathcal{P}_h$ and for any $\tilde{\mathbf{V}} \in \tilde{\mathbb{W}}$, which strictly enforces that:

$$\tilde{\Pi}\left(\mathfrak{D}_{\delta u}\left(\delta\mathbf{U}_h\right) + \mathfrak{B}\left(\delta\mathbf{U}_h\right) + \mathfrak{B}\left(\tilde{\mathbf{U}}\right)\right) = \tilde{\Pi}\left(\mathfrak{F} - \mathfrak{A}\left(\mathbf{U}_h^{n+1}\right) - \mathfrak{D}_t\left(\mathbf{U}_h^{n+1}\right)\right) \tag{52}$$

where $\tilde{\Pi}$ is the L^2 projection onto the space of subscales. This equation allows us to obtain an expression for the subscales:

$$\tilde{\Pi}\left(\mathfrak{B}\left(\tilde{\mathbf{U}}\right)\right) = \tilde{\Pi}\left(\mathfrak{R}\left(\delta\mathbf{U}_h, \mathbf{U}_h^{n+1}\right)\right) := \tilde{\Pi}\left(\mathfrak{R}_{\delta u}\left(\delta\mathbf{U}_h\right) + \bar{\mathfrak{R}}\left(\mathbf{U}_h^{n+1}\right)\right) \tag{53}$$

where $\mathfrak{R}_{\delta u}\left(\delta\mathbf{U}_h\right) := -\mathfrak{D}_{\delta u}\left(\delta\mathbf{U}_h\right) - \mathfrak{B}\left(\delta\mathbf{U}_h\right)$ and $\bar{\mathfrak{R}}\left(\mathbf{U}_h^{n+1}\right) := \mathfrak{F} - \mathfrak{A}\left(\mathbf{U}_h^{n+1}\right) - \mathfrak{D}_t\left(\mathbf{U}_h^{n+1}\right)$.

The idea now is to approximate operator $\mathfrak{B}$ by a matrix $\boldsymbol{\tau}_K^{-1}$ within each element K. Since we may consider that $\boldsymbol{\tau}_K^{-1}\tilde{\mathbf{U}}$ already belongs to the space of subscales, $\tilde{\Pi}\left(\boldsymbol{\tau}_K^{-1}\tilde{\mathbf{U}}\right) = \boldsymbol{\tau}_K^{-1}\tilde{\mathbf{U}}$, and from (53) we obtain:

$$\tilde{\mathbf{U}} \approx \boldsymbol{\tau}_K \tilde{\Pi}\left(\mathfrak{R}\left(\delta\mathbf{U}_h, \mathbf{U}_h^{n+1}\right)\right) \quad \text{in } K \in \mathcal{P}_h \tag{54}$$

where $\boldsymbol{\tau}_K$ is a matrix of algorithmic parameters depending on K and the operator $\mathfrak{B}$. This approximation for $\tilde{\mathbf{U}}$ is intended to mimic the effect of $\mathfrak{B}\left(\tilde{\mathbf{U}}\right)$ in the volume integral (46). Matrix $\boldsymbol{\tau}_K$ will be called the matrix of stabilization parameters. According to the heuristic approach proposed in [13] for the study of transient incompressible flows and its extension to material nonlinear problems in [11] we simplify the stabilization matrix by a diagonal one:

$$\boldsymbol{\tau}_K \approx \begin{pmatrix} \tau_u \mathbf{I} & \mathbf{0} \\ \mathbf{0} & \tau_p \end{pmatrix} \tag{55}$$

where τ_u and τ_p are coefficients coming from the study of the behavior of the stabilization parameters based on a Fourier analysis of the problem for the subscales. In this work, we propose to use the stabilization parameters proposed in [11] for linear elastic cases:

$$\tau_u = c_1 \frac{h_K^2}{2\mu} \quad \text{and} \quad \tau_p = 2c_2\mu \tag{56}$$

where c_1 and c_2 are algorithmic parameters which must be determined.

Finally, Eq. (54) can be introduced into the finite element scale equation (46) to obtain the following problem:

$$\begin{aligned}&\langle \mathbf{V}_h, \mathfrak{D}_{\delta u}(\delta \mathbf{U}_h)\rangle + \mathcal{B}(\delta \mathbf{U}_h, \mathbf{V}_h) + \sum_K \boldsymbol{\tau}_K \left\langle \mathfrak{L}(\mathbf{V}_h), \tilde{\Pi}\left(\mathfrak{R}\left(\delta \mathbf{U}_h, \mathbf{U}_h^{n+1}\right)\right)\right\rangle \\ &\quad = \mathcal{F}(\mathbf{V}_h) - \mathcal{A}\left(\mathbf{U}_h^{n+1}, \mathbf{V}_h\right) - \left\langle \mathbf{V}_h, \mathfrak{D}_t\left(\mathbf{U}_h^{n+1}\right)\right\rangle \quad \forall \mathbf{V}_h \in \mathbb{W}_{h,0}\end{aligned} \tag{57}$$

where $\mathfrak{L}(\mathbf{V}_h) = \left[\mathfrak{L}_u(\mathbf{V}_h), \mathfrak{L}_p(\mathbf{V}_h)\right]^T$ is a linear operator coming from the integration by parts of $\mathcal{B}$ such that $\mathcal{B}\left(\tilde{\mathbf{U}}, \mathbf{V}_h\right) = \sum_K \left\langle \mathfrak{L}(\mathbf{V}_h), \tilde{\mathbf{U}}\right\rangle_K$ and it is defined as:

$$\begin{aligned}\mathfrak{L}_u(\mathbf{V}_h)_a = &-\frac{\partial}{\partial X_A}\left\{\frac{\partial v_{h,a}}{\partial X_B} S'_{AB}\right\} + \frac{\partial}{\partial X_A}\left\{J p_h F^{-1}_{Aa}\frac{\partial v_{h,b}}{\partial X_B} F^{-1}_{Bb}\right\} \\ &- \frac{\partial}{\partial X_A}\left\{J p_h F^{-1}_{Ba}\frac{\partial v_{h,b}}{\partial X_B} F^{-1}_{Ab}\right\} - \frac{\partial}{\partial X_A}\left\{q f(J) F^{-1}_{Aa}\right\} \\ \mathfrak{L}_p(\mathbf{V}_h) = &\frac{\partial v_{h,a}}{\partial X_A} J F^{-1}_{Aa}\end{aligned} \tag{58}$$

There exist several stabilization methods coming from the VMS technique depending on the selection of the projection onto the subscales space. In this work, two different options are considered.

3.1. Algebraic subgrid scales (ASGS)

This is the simplest choice. We take the projection onto the subscales space as the identity when applied to the residual (see [36] for further details), so that

$$\tilde{\Pi}\left(\mathfrak{R}\left(\delta \mathbf{U}_h, \mathbf{U}_h^{n+1}\right)\right) = \mathfrak{R}\left(\delta \mathbf{U}_h, \mathbf{U}_h^{n+1}\right) = \mathfrak{R}_{\delta u}(\delta \mathbf{U}_h) + \bar{\mathfrak{R}}\left(\mathbf{U}_h^{n+1}\right) \tag{59}$$

and we obtain as a final stabilized formulation

$$\begin{aligned}&\langle \mathbf{V}_h, \mathfrak{D}_{\delta u}(\delta \mathbf{U}_h)\rangle + \mathcal{B}(\delta \mathbf{U}_h, \mathbf{V}_h) + \sum_K \boldsymbol{\tau}_K \langle \mathfrak{L}(\mathbf{V}_h), \mathfrak{R}_{\delta u}(\delta \mathbf{U}_h)\rangle = \mathcal{F}(\mathbf{V}_h) \\ &-\mathcal{A}\left(\mathbf{U}_h^{n+1}, \mathbf{V}_h\right) - \left\langle \mathbf{V}_h, \mathfrak{D}_t\left(\mathbf{U}_h^{n+1}\right)\right\rangle - \sum_K \boldsymbol{\tau}_K \left\langle \mathfrak{L}(\mathbf{V}_h), \bar{\mathfrak{R}}\left(\mathbf{U}_h^{n+1}\right)\right\rangle \quad \forall \mathbf{V}_h \in \mathbb{W}_{h,0}\end{aligned} \tag{60}$$

3.2. Orthogonal subgrid scales (OSS)

In [37] it is argued that a natural approximation for the unknown subgrid space is to take it orthogonal to the finite element space:

$$\tilde{\Pi}\left(\mathfrak{R}\left(\delta \mathbf{U}_h, \mathbf{U}_h^{n+1}\right)\right) = \mathfrak{R}\left(\delta \mathbf{U}_h, \mathbf{U}_h^{n+1}\right) - \Pi^h\left(\bar{\mathfrak{R}}\left(\mathbf{U}_h^{n+1}\right)\right) \tag{61}$$

where Π^h is the L^2 projection onto the finite element space. Due to the fact that this projection must increase the size of our system if we compute it in an implicit way, we have decided to approximate it with the residual of the previous time step by neglecting the projection of the operator $\mathfrak{R}_{\delta u}(\delta \mathbf{U}_h)$. The final form of the stabilized problem with OSS method emerges as:

$$\begin{aligned}&\langle \mathbf{V}_h, \mathfrak{D}_{\delta u}(\delta \mathbf{U}_h)\rangle + \mathcal{B}(\delta \mathbf{U}_h, \mathbf{V}_h) + \sum_K \boldsymbol{\tau}_K \langle \mathfrak{L}(\mathbf{V}_h), \mathfrak{R}_{\delta u}(\delta \mathbf{U}_h)\rangle \\ &\quad = \mathcal{F}(\mathbf{V}_h) - \mathcal{A}\left(\mathbf{U}_h^{n+1}, \mathbf{V}_h\right) - \left\langle \mathbf{V}_h, \mathfrak{D}_t\left(\mathbf{U}_h^{n+1}\right)\right\rangle \\ &\quad + \sum_K \boldsymbol{\tau}_K \left\langle \mathfrak{L}(\mathbf{V}_h), \Pi^h\left(\bar{\mathfrak{R}}\left(\mathbf{U}_h^{n+1}\right)\right) - \bar{\mathfrak{R}}\left(\mathbf{U}_h^{n+1}\right)\right\rangle \quad \forall \mathbf{V}_h \in \mathbb{W}_{h,0}\end{aligned} \tag{62}$$

Remark 3.3. A key property of the OSS stabilization is that, thanks to the projection onto the finite element space, we keep the consistency of the formulation in a weakly sense in spite of including just the minimum number of terms to stabilize the solution.

4. Numerical examples

In this section, several numerical examples are presented to assess the performance of the proposed formulation. The first case we consider is a test with a manufactured solution in order to analyze the spatial discretization errors with respect to the mesh size. Later, we evaluate the performance of our finite element formulation in the incompressible limit through the standard Cook's membrane test. The third case we consider is a bending problem for a beam-like structure in order to show the behavior of the method in incompressible bending dominated scenarios. Finally, a twisting column is set which presents extreme nonlinear deformations. All these examples are widely used in incompressible hyperelastic cases [24,25,27,28].

For all the numerical examples included next, hyperelastic models are considered fully incompressible, and so the bulk modulus is $\kappa = \infty$. The algorithmic parameters are set to $c_1 = 1$ and $c_2 = 1$. As previously discussed, the nonlinearities in the problem are solved via a Newton–Raphson scheme. Depending on the nonlinearities, the initial guess of the iterative procedure needs to be close enough to the solution to guarantee convergence of the nonlinear iterations. In time-depending schemes, the time step is the parameter which controls the evolution of the nonlinear iterations, so we will have to tune it depending on the nonlinearities of each numerical example. A maximum of 10 iterations is set, and the numerical tolerance for the L^2 norm is 10^{-7}. In order to solve the monolithic system of linear equations, we use the Biconjugate Gradients solver, `BiCGstab` [38], which is already implemented in the `PETSc` parallel solver library [39].

Remark 4.1. Some works prefer to choose the time step size based on either the characteristic shear wave speed or the stabilization parameter size. We prefer not to use this approach since it mixes the definition of the stabilization parameter with the time discretization of the problem.

4.1. A test with analytical solution

Let us first perform a simple test whose main objective is to numerically check the order of convergence of the proposed scheme with respect to the mesh size. For this purpose we use the so-called method of manufactured solutions.

In this procedure, an exact analytical solution is defined a priori and later substituted into the continuum equations in order to obtain associated forcing terms. These forcing terms are then introduced as perturbations in the finite element computation. The manufactured solutions are composed of smooth functions. Dirichlet boundary conditions are prescribed over the boundaries upon evaluation of the displacement analytical solution. So as to avoid mixing both spatial and time errors, we consider static solutions.

The region we consider is the unit square plate $\Omega_0 = [0, 1] \times [0, 1]$ m^2 under plain strain and we impose the following manufactured displacement field

$$\boldsymbol{u}(X, Y) = k \left[(X + Y)^2 \exp(X + Y), -(X + Y)^2 \exp(X + Y) \right] \tag{63}$$

$$p(X, Y) = \frac{E}{3} \sin(2\pi X) \sin(2\pi Y) \tag{64}$$

where $k = 0.01$ m^{-1} and X and Y referring to the Cartesian axes in the reference configuration (cf. Figs. 1a, 1b and 1c).

It is important to note that this displacement field gives an incompressible motion due to the fact that the Jacobian $J = 1$ for all X, Y. We set a neo-Hookean material with quadratic law for the deviatoric part of the stresses, with Young Modulus $E = 10$ MPa. We study the convergence behavior of the proposed method by running the case on seven meshes obtained by refinement of the grid shown in 1d. The sequence is of structured grids of $2 \times n^2$ linear elements, being n the number of finite elements along each side of the domain.

The normalized error has been computed in the L^2-norm for displacement and pressure with ASGS and OSS stabilization techniques. Figs. 2a and 2b show the convergence plot for the proposed algorithm. The reader can note that the scheme proposed shows the desired rate of convergence regardless of the stabilization technique.

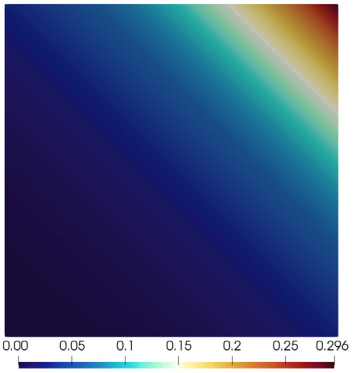

(A) Displacement u_x(m)

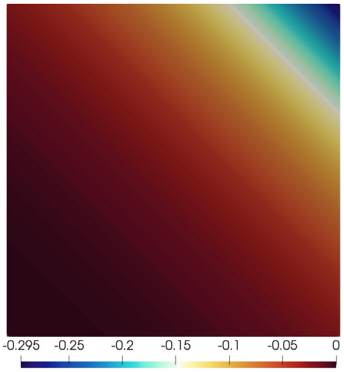

(B) Displacement u_y(m)

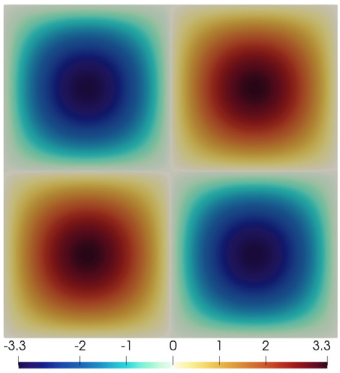

(C) Pressure p (MPa)

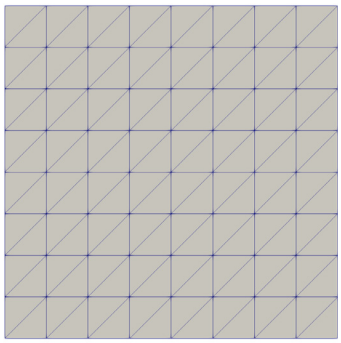

(D) Structured Mesh

Fig. 1. Manufactured convergence test. Displacement and Pressure solutions 1a, 1b and 1c and an example of a linear triangular structured mesh 1d.

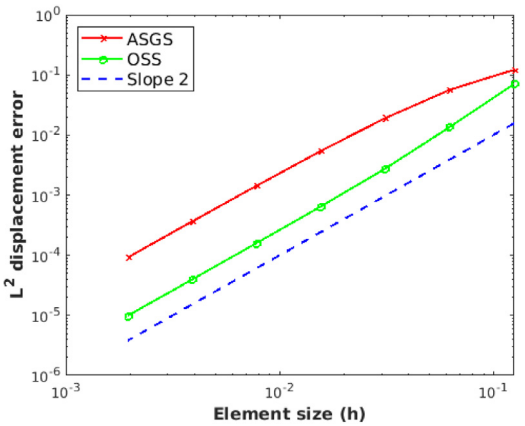

(A) L^2 Displacement error

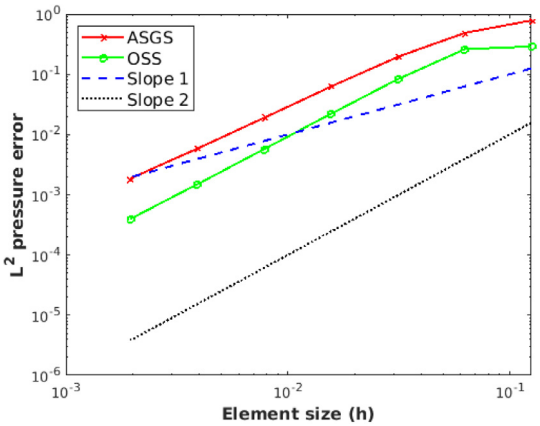

(B) L^2 Pressure error

Fig. 2. Manufactured convergence test. L^2 errors.

4.2. Plane strain Cook's membrane

In this case, we study the dynamic Cook's membrane, a bending dominated example. This is the standard test used by many authors as a reference test to check their formulations. Although this test was firstly introduced for

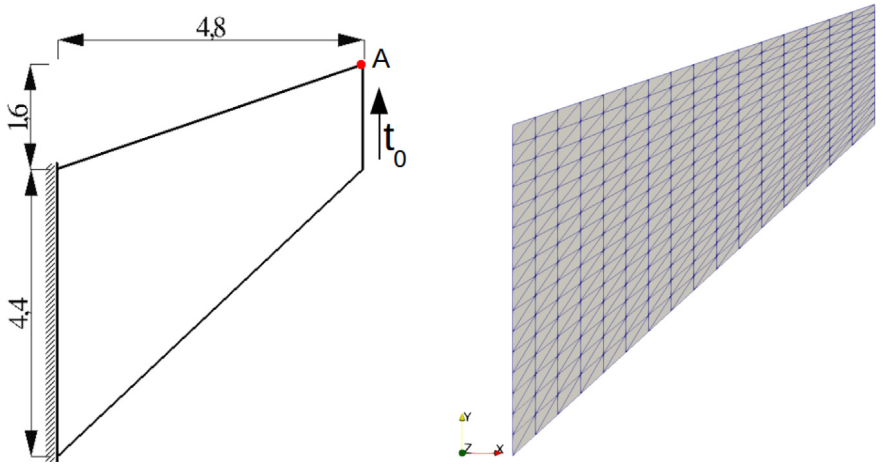

(A) Geometry (m)

(B) Linear triangular mesh with N finite elements along each side

Fig. 3. Cook's membrane problem. Geometry (3a) and an example of a linear triangular mesh (3b).

static cases [10,27], an extension to transient problems can be found in [28]. We are going to keep the finite strain assumption in order to evaluate our nonlinear finite element formulation, even if in this case the strains could be considered small.

The problem consists of a tapered panel, clamped on the left side and subjected to a shearing vertical load at the free right edge, $\mathbf{t}_0 = (0, 6.25)$ Pa. Stress free boundary conditions are applied on the remaining boundaries. We set a neo-Hookean material with Young Modulus $E = 250$ Pa and density $\rho_0 = 1$ kg/m^3. To define the deviatoric part of the material, we consider a Quadratic law. The initial conditions are $\mathbf{u}^0 = \mathbf{0}$ and $\mathbf{v}^0 = \mathbf{0}$. The geometry of this problem is shown in 3a.

In order to test the evolution of the solution while refining our mesh, the problem has been discretized into linear triangular structured meshes with N finite elements along each side (see Fig. 3b).

In Fig. 4, we present a comparison of the vertical displacement at point A at $t = 7$ s using the mixed formulation without stabilization and stabilized with both the ASGS and the OSS methods. For all cases, we fix the time step as $\delta t = 0.05$ s and the BDF2 time integration scheme is applied.

Remark 4.2. In this case, we have selected BDF2 in order to ensure that the numerical dissipation introduced by the time integration scheme is enough to eliminate the nonphysical high-frequency modes appearing in the numerical solution (see Fig. 6).

Fig. 4 illustrates the convergence of our mixed proposed formulation depending on the chosen stabilization. Both OSS and ASGS deal appropriately with the incompressibility constraint whereas when no stabilization is considered we observe a poor convergence rate. Despite the fact that the momentum equation does not need to be stabilized, the error introduced for the constitutive law of the pressure causes the poor accuracy of the displacement. As expected, the proposed stabilized mixed formulation does not exhibit volume locking for neither the ASGS nor the OSS methods.

It is interesting to observe that the ASGS stabilization method behaves better than the OSS one only for really coarse meshes. This behavior is justified due to the fact that in the OSS technique, we are approximating the projection onto the finite element space evaluated in the previous time step. This approximation may be introducing an error that clearly depends on the mesh as well as the time step size.

For the sake of completeness, Fig. 5 shows the pressure field for the three cases and the deformed solution at $t = 7$ s. As mentioned before, when no stabilization is applied, pressure gradients appear over the inner element boundaries due to the jumps of pressure values in the elements as it can be observed in Fig. 5a. On the other hand,

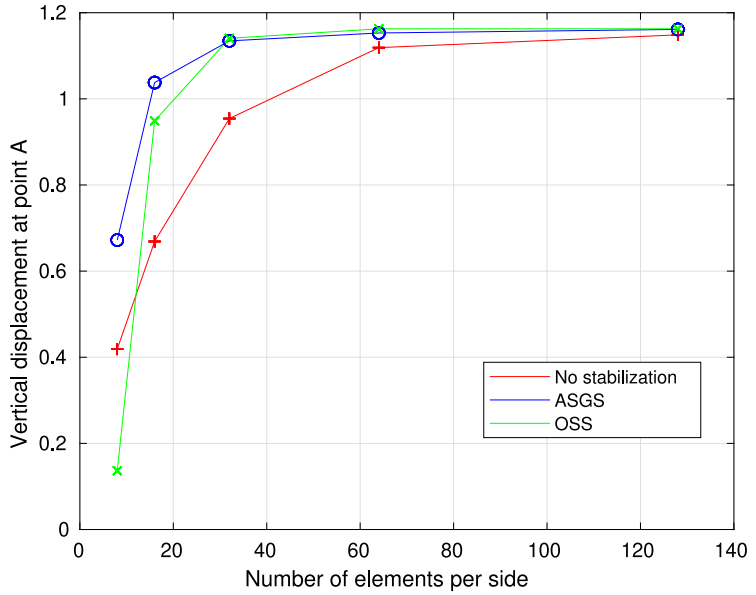

Fig. 4. Cook's membrane problem. Convergence of the vertical displacement (m) at point A at $t = 7$ s.

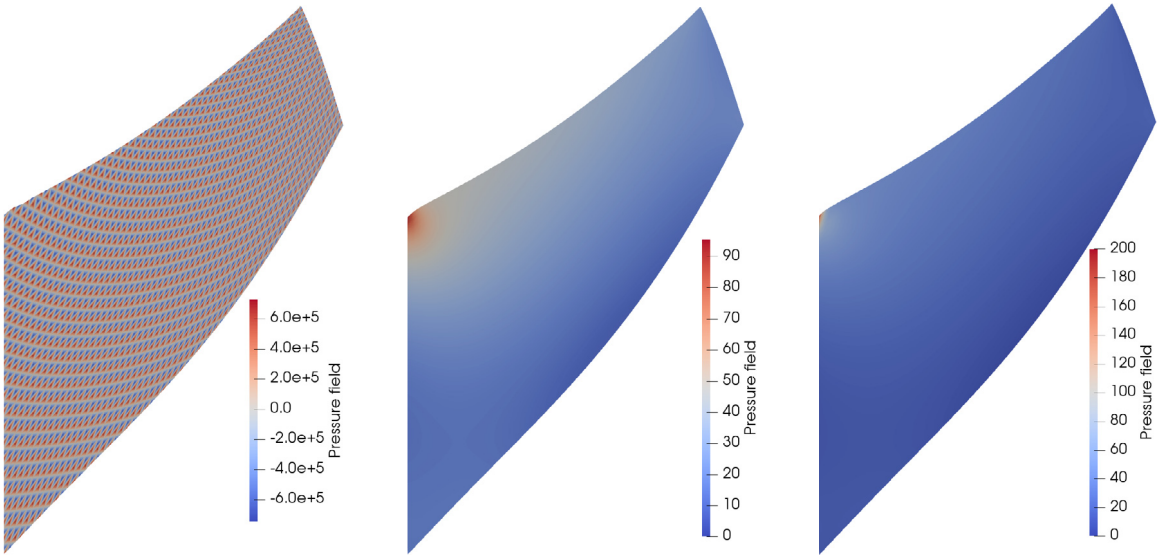

(A) No Stabilization (B) ASGS (C) OSS

Fig. 5. Cook's membrane problem. Pressure field (Pa) for a 64 × 64 × 2 triangular linear mesh.

we can see that both the ASGS and the OSS methods yield the pressure field properly, as it is shown in Figs. 5b and 5a. Let us remark that the OSS method is able to concentrate more accurately the maximum values of the pressure.

In order to study the relation between the different proposed formulations with the several time integration schemes we have introduced in this work, we show in Fig. 6 the evolution up to $T = 7$ s of both the vertical displacement and the pressure at the right top corner of the membrane for $\delta t = 0.05$ s and for a fixed 128 × 128 × 2 linear triangular mesh.

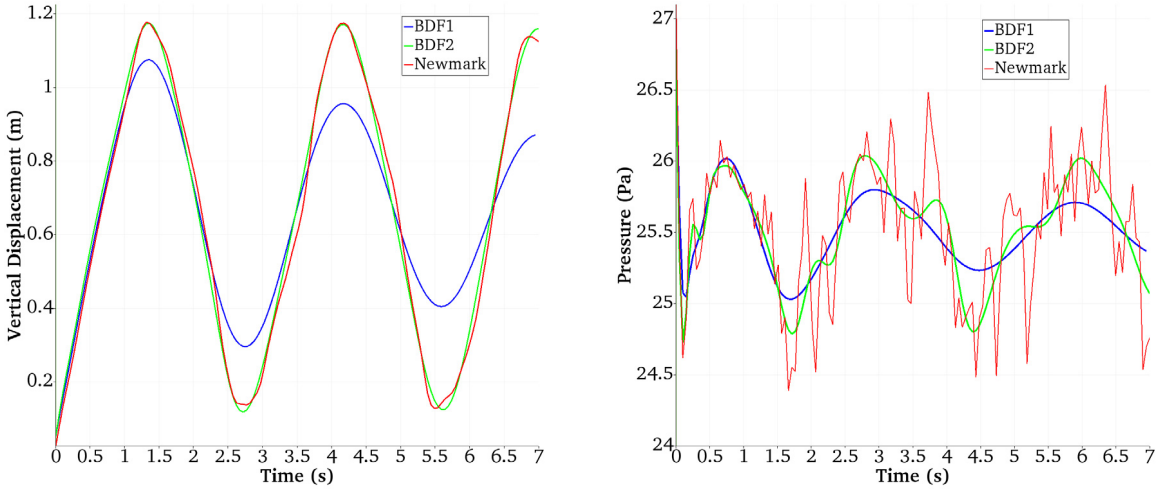

(A) Vertical Displacement (m) (B) Pressure (Pa)

Fig. 6. Cook's membrane problem. Comparison between several time integrators with $\delta t = 0.05$ s and a linear triangular mesh with 128 elements per side.

The comparison of the BDF1, the BDF2 and the Newmark time integrators of Fig. 6 clearly demonstrates the following facts. On the one hand, BDF1 is only first-order accurate and it is highly dissipative, affecting the accuracy of the method by eliminating physical modes of the pressure. On the other hand, in spite of the fact that Newmark scheme is second-order for $\beta = \frac{1}{4}$ and $\gamma = \frac{1}{2}$, it does not introduce any numerical dissipation, which would help preventing high frequency oscillations of unphysical modes. With regard to BDF2, it is seen that it is able to dissipate the nonphysical modes while keeping the accuracy of the method and it can be safely used.

Remark 4.3. In order to overcome the problem described with the Newmark scheme, several time integrators have been introduced over last decades, including the Generalized-α method [40], to control the numerical dissipation that needs to be added to the system.

4.3. A 3D bending beam problem

As a third test in finite elasticity, we consider a three dimensional beam of square section clamped on its bottom face very similar to the one presented in [27]. The initial geometry is a parallelepiped of dimension $1 \times 1 \times 6$ m as shown in Fig. 7a. We consider stress free conditions and zero displacement initial conditions are applied. In order to initialize the bending of the column, we impose an initial velocity condition Fig. 7b and an initial displacement field such that:

$$\mathbf{v}^0(x, y, z) = \left(\frac{5}{3}z, 0, 0\right)^T \quad \text{m/s} \quad ; \quad \mathbf{u}^0(x, y, z) = \mathbf{0} \quad \text{m} \tag{65}$$

The material is considered Mooney–Rivlin with initial density $\rho_0 = 1.1 \times 10^3$ kg/m^3, $\alpha_1 = 0.182$ MPa and $\alpha_2 = 9.79 \times 10^{-3}$ MPa, identical to the one proposed in [28]. Due to the fact that the beam is clamped on its bottom face, we impose homogeneous boundary conditions for the displacement field. The rest of the boundary is prescribed with zero traction.

The interest of this example is to show the performance of the proposed formulation in bending dominated scenarios. As explained before, this method is independent of the kind of hyperelastic material model. Therefore, we have selected a Mooney–Rivlin model to simulate this bending dominated problem. The main goal of this example is to show that our stabilized mixed formulation works properly in bending dominated scenarios and in 3D cases for truly incompressible materials. For this reason, we have selected 3 different linear tetrahedral meshes,

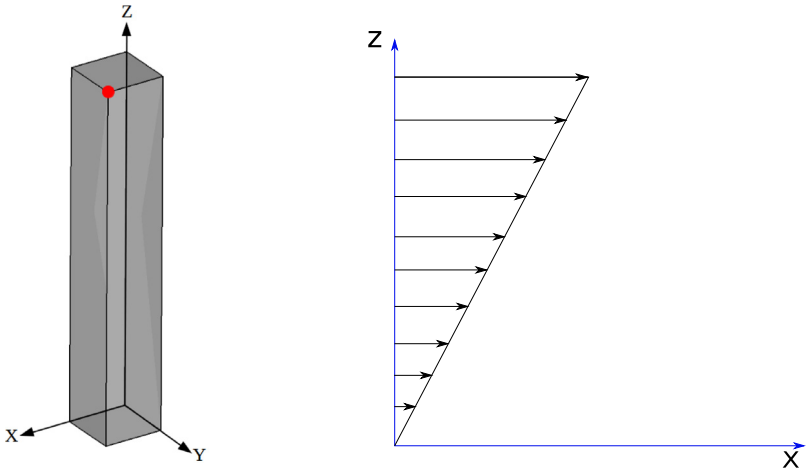

(A) Geometry (B) Initial Velocity, $\mathbf{v}(x, y, z, t = 0)$

Fig. 7. Bending beam. Geometry (7a) and initial velocity field (7b).

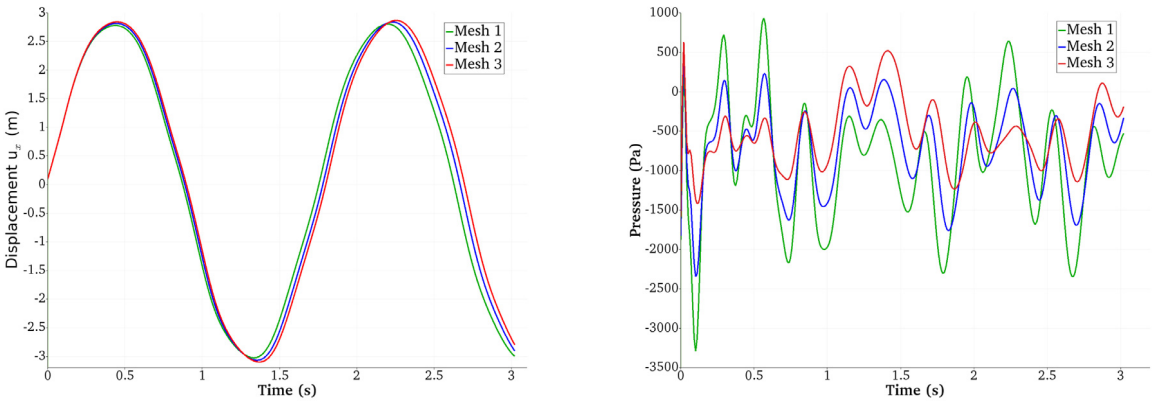

(A) Displacement u_x (m) (B) Pressure (Pa)

Fig. 8. Bending beam. Comparison between several meshes with $\delta t = 0.01$ s and ASGS as stabilization technique.

which are built from original meshes made of hexahedra further subdivided into 6 tetrahedra:

Mesh	Number of elements
1	$6 \times 6 \times 36 \times 6$
2	$8 \times 8 \times 48 \times 6$
3	$12 \times 12 \times 72 \times 6$

In order to avoid unphysical modes appearing from the time integration scheme, we have selected the high-dissipative BDF2 time integrator with time step $\delta t = 0.01$ s.

Fig. 8 displays a comparison among several refinement levels up to $T = 3$ s at the red point of Fig. 7a. Fig. 8 clearly shows the effectiveness of the proposed scheme to produce locking-free behavior without spurious oscillations in the pressure field. It is interesting to see that even for very coarse meshes like Mesh 1, where the

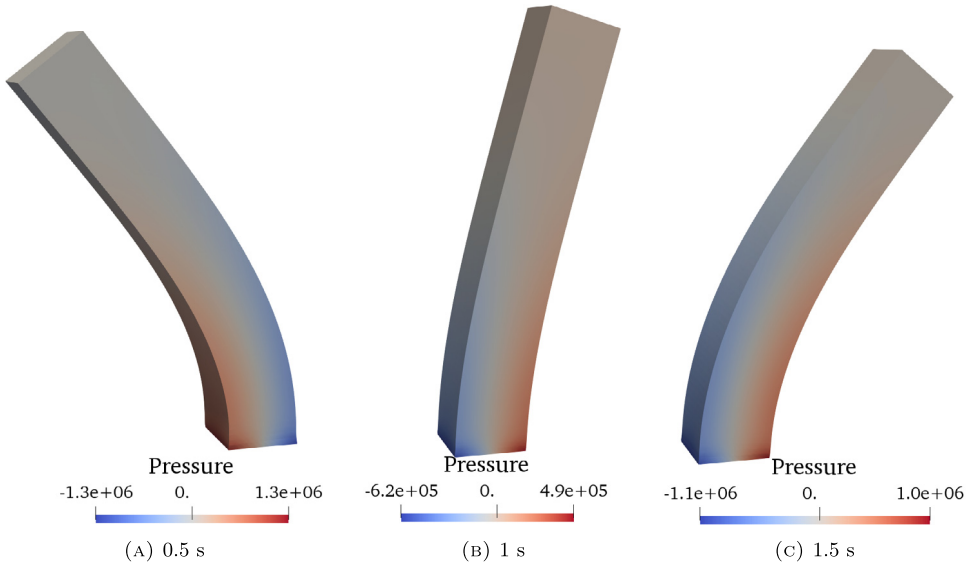

(A) 0.5 s (B) 1 s (C) 1.5 s

Fig. 9. Bending beam. Deformation and pressure field (Pa) for $\delta t = 0.01$ s with ASGS stabilization technique.

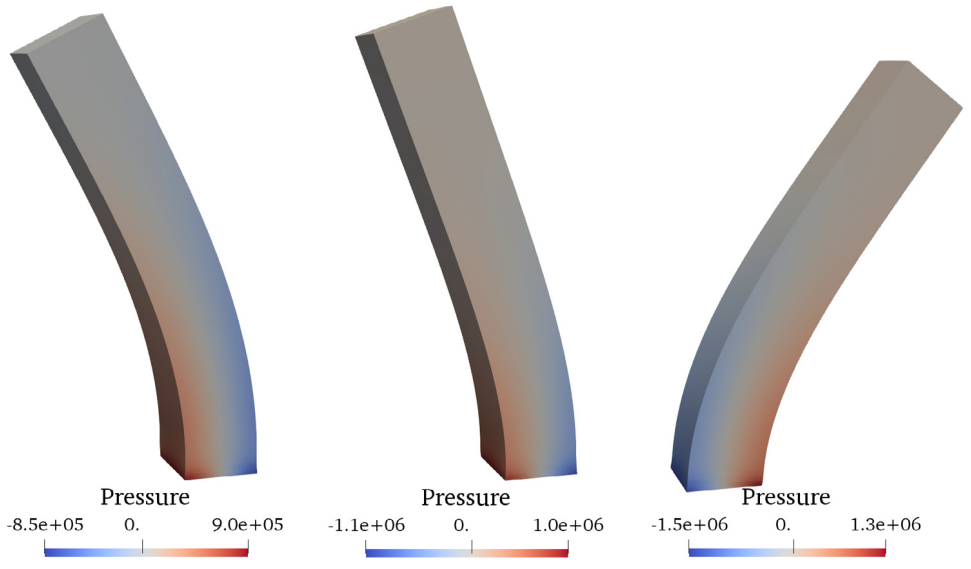

(A) 2 s (B) 2.5 s (C) 3 s

Fig. 10. Bending beam. Deformation and pressure field for $\delta t = 0.01$ s with ASGS stabilization technique.

spatial error is propagated along time, the method is able to capture well-solved fields without unphysical modes in the pressure field.

To end up this problem, Figs. 9 and 10 show the evolution of the deformation and the pressure field along time up to $T = 3$ s for Mesh 3. It can be observed that the deformation is accurately reproduced even for complex hyperelastic material models like the Mooney–Rivlin model in fully incompressible scenarios. Regarding the pressure field, we can state that it is correctly captured by our mixed formulation, placing the maximum values of the pressure at the bottom of the beam, where the structure is clamped and where they are expected to appear.

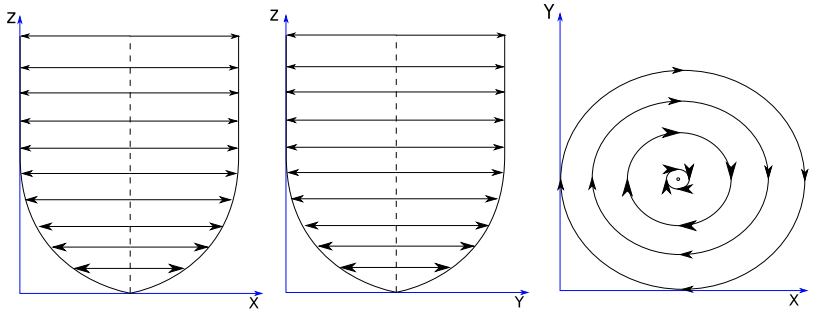

Fig. 11. Twisting column. Initial Velocity Field.

4.4. Twisting column

As a final example, we present the twisting column test. This test is widely used to assess the robustness of any formulation in extreme nonlinear deformations [24,25,27,28].

The geometry is identical to the bending beam described in the previous example. The beam is also clamped on its bottom face. In order to make the column twist, we apply an initial sinusoidal velocity field:

$$\mathbf{v}^0\,(x, y, z) = \Omega\ \sin\left(\frac{\pi z}{12}\right)(y, -x, 0)^T \quad \text{m/s} \tag{66}$$

The material is considered neo-Hookean with initial density $\rho_0 = 1.1\times10^3$ kg/m^3, Young modulus $E = 1.7\times10^7$ Pa and Poisson ratio $\nu = 0.5$. To define the deviatoric part of the material, we consider a Simo–Taylor law. The geometry of the column is shown in Fig. 7a and the applied initial velocity in Fig. 11. Several levels of refinement have been considered to perform the computations. To construct the meshes, we start with hexahedral elements which are further subdivided into 6 tetrahedral ones each. So we consider 3 different meshes. Mesh 1, with $8 \times 8 \times 48 \times 6$ linear finite elements, Mesh 2 with $12 \times 12 \times 72 \times 6$ elements and we end up with Mesh 3 with $16 \times 16 \times 96 \times 6$ elements. We consider the BDF2 time integrator.

The deformation and the pressure field are shown for $t = 0.1$ s and $t = 0.3$ s in Figures Figs. 12, 13 and Figs. 14, 15 respectively. We have included the results for $\delta t = 0.01$ s and $\delta t = 0.001$ s in order to observe the roll of the time step.

With regard to the time step, we can observe that Figs. 13 and 15 are able to locate the maximum and minimum values of the pressure in the more stressed areas, in this case, near to the clamped boundary. It is interesting to observe that the mixed formulation proposed here produces a smooth and accurate pressure field for the fully incompressible case. Let us also remark that for coarse meshes, we observe a spatial error which is propagated along time causing the difference in the deformation that we can appreciate in Figures 14 and 15.

Clearly, our stabilized mixed implementation produces locking-free solutions and it does not exhibit non-physical pressure fluctuations thanks to both the application of BDF2, a high-frequency dissipation time integrator, and the application of VMS stabilization technique, which include sufficient numerical stabilization to the problem.

In Fig. 16, we consider a comparison of the ASGS and OSS stabilization techniques of the mixed formulation for Mesh 3 and $\delta t = 0.001$ s. Both stabilizations seem to closely track each other, also considering the fact that the OSS technique is more dependent of the time step size due to the approximation in the computation of the projection onto the finite element space, which is computed in the previous time step to save computational effort. According to the solutions presented in [27], the displacement field is correctly captured with both stabilization methods.

Fig. 17 shows the evolution of the deformation of the twisting column along time up to $T = 0.5$ s for Mesh 3 and with $\delta t = 0.001$ s and using the ASGS stabilization method. It is easy to observe the well-reproduced evolution of the deformation of the column. Taking into account that this example is considered very challenging due to the extreme nonlinear deformations and huge number of pressure modes that appear, we remark the robustness and applicability of our stabilized mixed formulation.

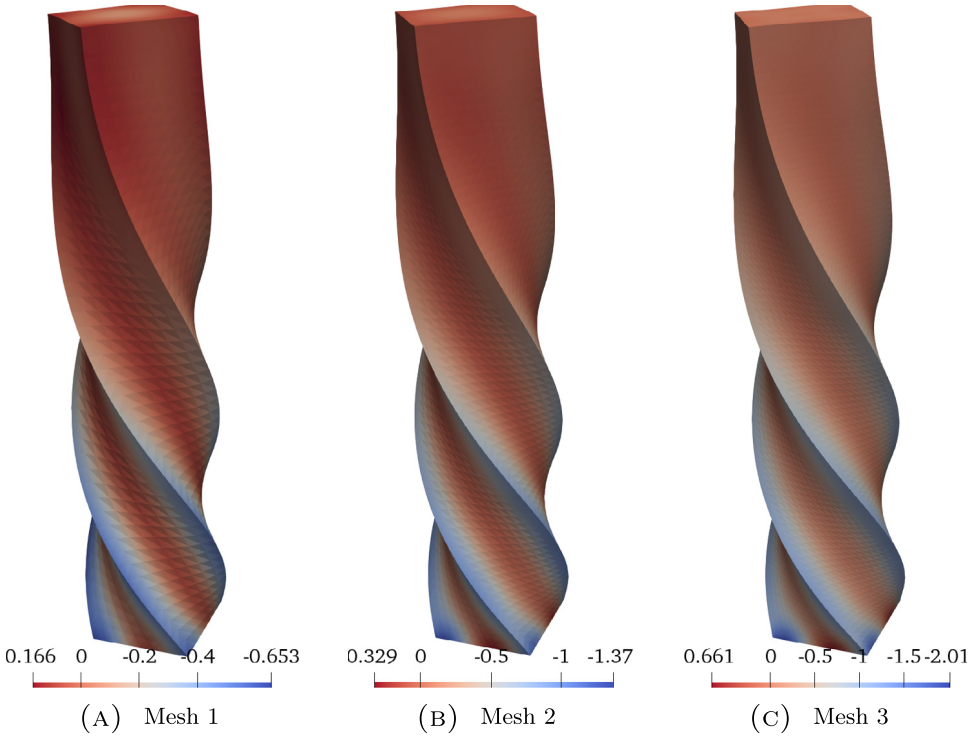

Fig. 12. Twisting column. Deformation and pressure field (MPa) for $\delta t = 0.01$ s at $t = 0.1$ s with the OSS stabilization technique.

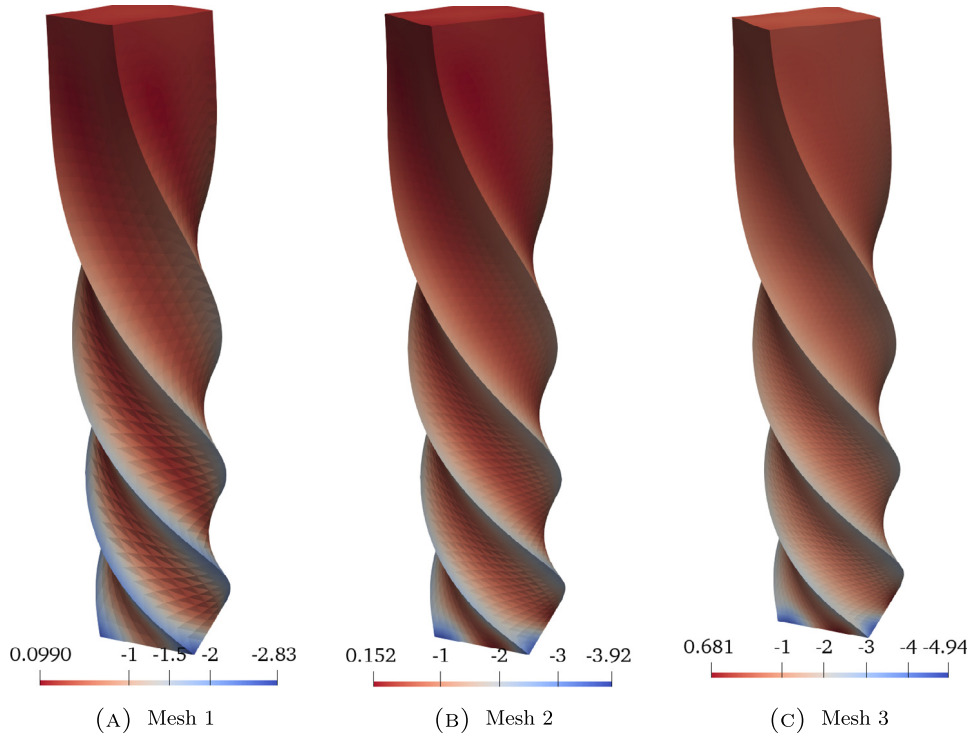

Fig. 13. Twisting column. Deformation and pressure field (MPa) for $\delta t = 0.001$ s at $t = 0.1$ s with the OSS stabilization technique.

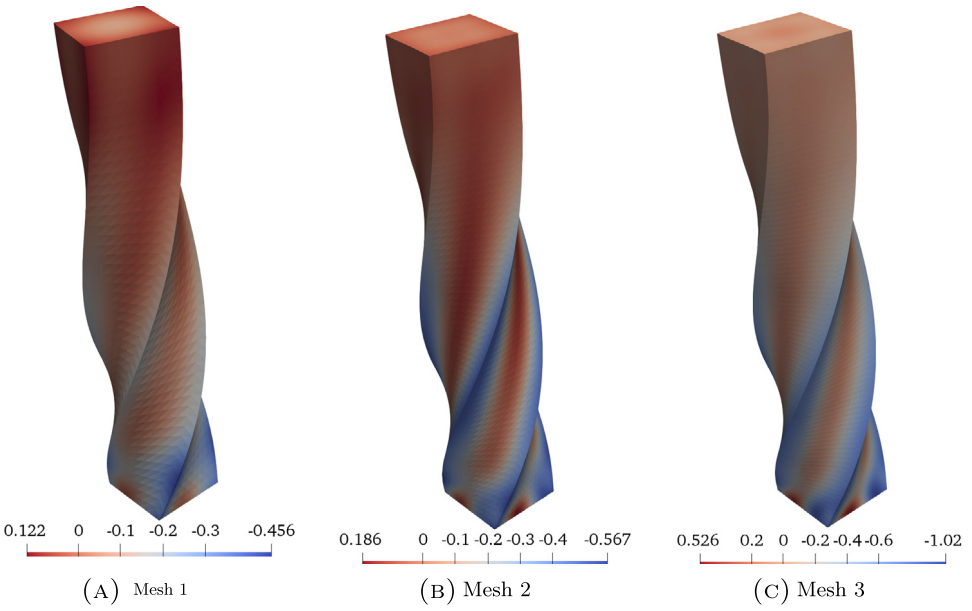

Fig. 14. Twisting column. Deformation and pressure field (MPa) for $\delta t = 0.01$ s at $t = 0.3$ s with the OSS stabilization technique.

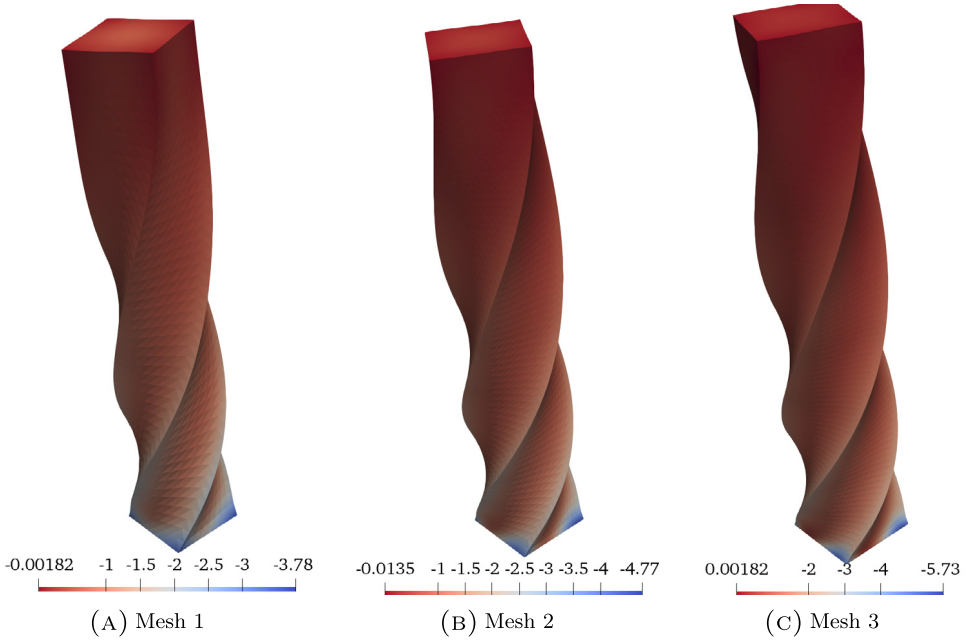

Fig. 15. Twisting column. Deformation and pressure field (MPa) for $\delta t = 0.001$ s at $t = 0.3$ s with the OSS stabilization technique.

To end up this problem, Fig. 18 displays the nonlinear iteration convergence at time $t = 0.5$ s for Mesh 3 and with $\delta t = 0.001$ s. The method shows almost quadratic convergence no matter the stabilization technique we are applying. It is important to remark some stabilization terms have been linearized only up to first order, as the finite element projections in the OSS method.

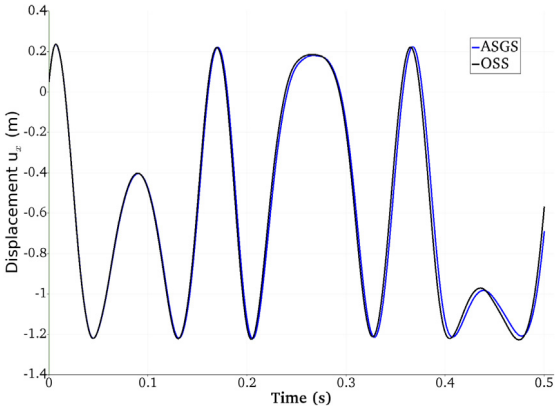

(A) Displacement u_x

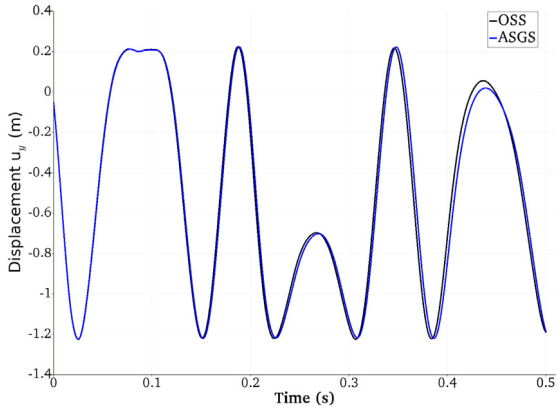

(B) Displacement u_y

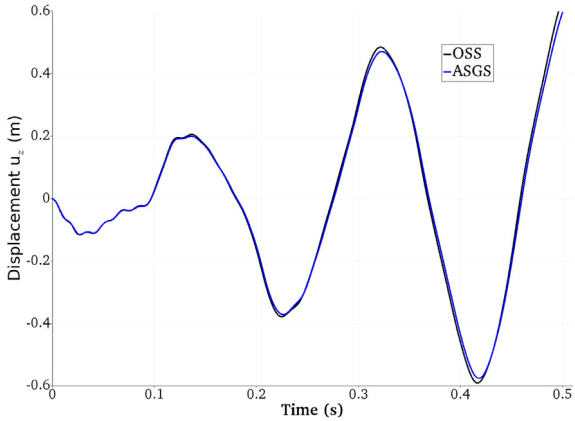

(C) Displacement u_z

Fig. 16. Twisting column. Displacement field at point A.

5. Conclusions

In this paper we have described a new simple stabilized finite element method for the study of solid dynamics when considering nearly and fully incompressible materials. The point of departure is the splitting of the Cauchy stress tensor into deviatoric and spherical components, which then translates into a splitting of the second Piola–Kirchhoff stress tensor.

Regarding the constitutive law, we have presented a formulation which works properly for any hyperelastic material model in which the strain energy function can be decomposed in deviatoric and volumetric parts, the latter in terms of the bulk modulus, κ. We have taken advantage of this decomposition to obtain a constitutive law for the pressure from the volumetric part. This law is formulated properly to obtain a simple way to impose the incompressibility of the material automatically. The resulting equation has been added to the momentum equation to obtain a monolithic system of equations for the displacement/pressure pair.

With regard to the time integration scheme, we have shown that although any time integrator can be applied, implicit high-frequency dissipation time integration schemes are more suitable. To avoid pressure fluctuations of our solution along time, high-frequency dissipation schemes are recommended.

In Section 3 we have proposed a residual-based stabilization technique based on the decomposition of the unknowns into finite element scales and subgrid scales. Unlike the standard VMS stabilization technique, we have proposed to use the OSS formulation. In this approach the subgrid scale space is supposed to be perpendicular to

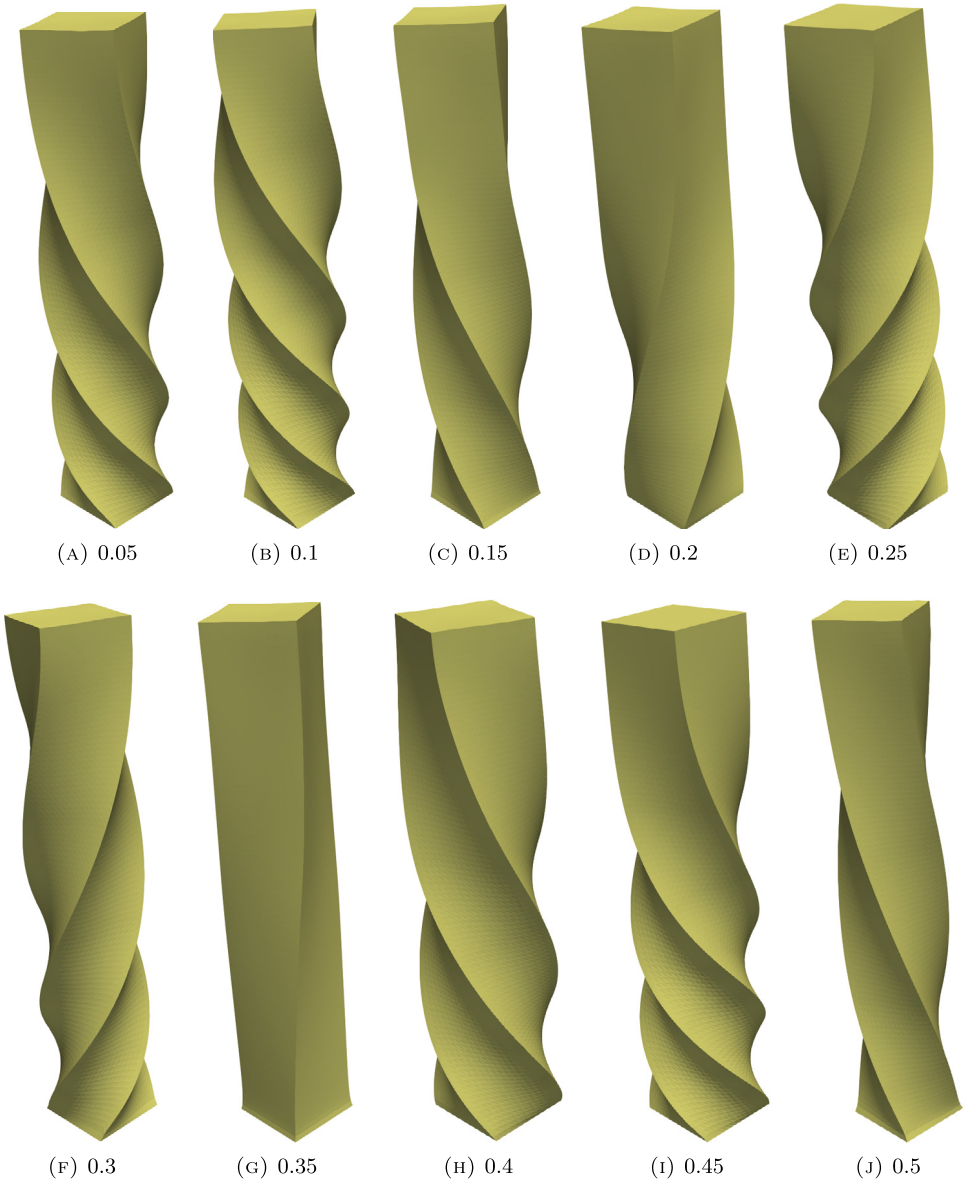

Fig. 17. Twisting column. Deformation along time (in s).

the finite element one. As shown in Section 4, this stabilization exhibits better accuracy than the classical ASGS method for a fixed mesh. A key point is the way we have selected the stabilization parameters, where we have decided to give a closed-form expression based on previous works. We have shown also that the approximation of considering the subgrid scales to be modeled as bubble functions does not pollute the solution. Likewise, for the examples we have considered, we have been able to assume quasi-static subscales, although dynamic subscales might need to be considered if very small time step sizes are used.

Concerning the computational cost of the method, we have observed that the methods proposed display (almost) quadratic non-linear convergence, as it is expected from the implementation of a Newton–Raphson iterative procedure. The number of unknowns is only increased by one per each node with respect to the classical irreducible displacement-based formulation, which is the minimum to be able to enforce incompressibility.

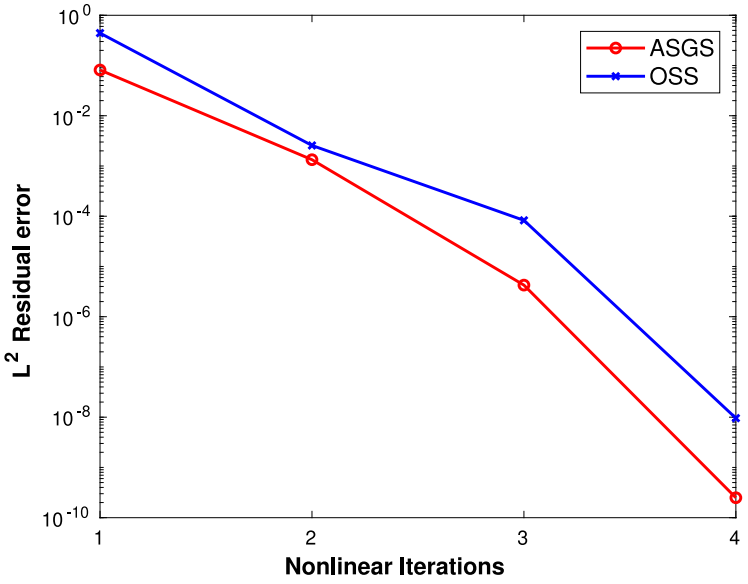

Fig. 18. Twisting column. Nonlinear iteration convergence at $t = 0.5$ s.

Declaration of competing interest

The authors declare that they have no known competing financial interests or personal relationships that could have appeared to influence the work reported in this paper.

Acknowledgments

Inocencio Castañar gratefully acknowledges the support received from the Agència de Gestió d'Ajut i de Recerca through the predoctoral FI grant 2019-FI-B-00649. J. Baiges gratefully acknowledges the support of the Spanish Government through the Ramón y Cajal grant RYC-2015-17367. R. Codina gratefully acknowledges the support received through the ICREA Acadèmia Research Program of the Catalan Government. This work was partially funded through the TOP-FSI: RTI2018-098276-B-I00 project of the Spanish Government.

References

[1] G.A. Holzapfel, Nonlinear Solid Mechanics. A Continuum Approach for Engineering, Wiley, 2000.
[2] G.A. Holzapfel, Biomechanics of soft tissue, Handb. Mater. Behav. 3 (2001) 1049–1063.
[3] T. Belytschko, W.K. Liu, B. Moran, Nonlinear Finite Elements for Continua and Structures, Wiley, 2001.
[4] T.J.R. Hughes, The Finite Element Method: Linear Static and Dynamic Finite Element Analysis, Prentice-Hall, Englewood Cliffs, New Jersey, 1987.
[5] I. Babuška, Error-bounds for finite element method, Numer. Math. 16 (4) (1971) 322–333.
[6] D.S. Malkus, T.J.R. Hughes, Mixed finite element methods - Reduced and selective integration techniques: A unification of concepts, Comput. Methods Appl. Mech. Engrg. 15 (1978) 63–81.
[7] T.J.R. Hughes, L.P. Franca, M. Balestra, A new finite element formulation for computational fluid dynamics: V. Circumventing the babuška-brezzi condition: a stable Petrov-Galerkin formulation of the stokes problem accommodating equal-order interpolations, Comput. Methods Appl. Mech. Engrg. 59 (1986) 85–99.
[8] R. Codina, A stabilized finite element method for generalized stationary incompressible flows, Comput. Methods Appl. Mech. Engrg. 190 (2001) 2681–2706.
[9] L.P. Franca, T.J.R. Hughes, A.F.D. Loula, I. Miranda, A new family of stable elements for nearly incompressible elasticity based on a mixed Petrov-Galerkin finite element formulation, Numer. Math. 53 (1–2) (1988) 123–141.
[10] M. Chiumenti, Q. Valverde, C.A. de Saracibar, M. Cervera, A stabilized formulation for incompressible elasticity using linear displacement and pressure interpolations, Comput. Methods Appl. Mech. Engrg. 191 (2002) 1095–1116.
[11] M. Cervera, M. Chiumenti, R. Codina, Mixed stabilized finite element methods in nonlinear solid mechanics. Part I: Formulation, Comput. Methods Appl. Mech. Engrg. 199 (37–40) (2010) 2559–2570.
[12] M. Cervera, M. Chiumenti, R. Codina, Mixed stabilized finite element methods in nonlinear solid mechanics. Part II: Strain localization, Comput. Methods Appl. Mech. Engrg. 199 (37–40) (2010) 2571–2589.

[13] R. Codina, Stabilized finite element approximation of transient incompressible flows using orthogonal subscales, Comput. Methods Appl. Mech. Engrg. 191 (2002) 4295–4321.
[14] R. Codina, J.M. González-Ondina, G. Díaz-Hernández, J. Príncipe, Finite element approximation of the modified Boussinesq equations using a stabilized formulation, Int. J. Numer. Methods Eng. 57 (2008) 1249–1268.
[15] T.J.R. Hughes, G.R. Feijóo, L. Mazzei, J. Quincy, The variational multiscale method - a paradigm for computational mechanics, Comput. Methods Appl. Mech. Engrg. 166 (1998) 3–24.
[16] M. Chiumenti, M. Cervera, R. Codina, A mixed three-field FE formulation for stress accurate analysis including the incompressible limit, Comput. Methods Appl. Mech. Engrg. 283 (2015) 1095–1116.
[17] J. Bonet, A.J. Burton, A simple average nodal pressure tetrahedral element for incompressible and nearly incompressible dynamic explicit applications, Comput. Methods Appl. Mech. Engrg. 1 (4) (1998) 437–449.
[18] C.H. Lee, A.J. Gil, J. Bonet, Development of a cell centred upwind finite volume algorithm for a new conservation law formulation in structural dynamics, Comput. Struct. 118 (2013) 13–38.
[19] M. Aguirre, A.J. Gil, J. Bonet, A. Arranz-Carreño, A vertex centred finite volume Jameson-Schmidt-Turkel (JST) algorithm for a mixed conservation formulation in solid dynamics, J. Comput. Phys. 259 (2014) 672–699.
[20] C.H. Lee, J. Haider, A.J. Gil, J. Bonet, A first-order hyperbolic framework for large strain computational solid dynamics. An upwind cell centred Total Lagrangian scheme, Internat. J. Numer. Methods Engrg. 109 (2017) 407–456.
[21] C.H. Lee, A.J. Gil, J. Bonet, Development of a stabilised Petrov-Galerkin formulation for linear tetrahedral elements in compressible, nearly incompressible and truly incompressible fast dynamics, Comput. Methods Appl. Mech. Engrg. 268 (2014) 40–64.
[22] C.H. Lee, A.J. Gil, J. Bonet, M. Aguirre, A stabilised Petrov-Galerkin formulation for linear tetrahedral elements in compressible, nearly incompressible and truly incompressiblefast dynamics, Comput. Methods Appl. Mech. Engrg. 276 (2014) 659–690.
[23] M. Aguirre, A.J. Gil, J. Bonet, C.H. Lee, An upwind vertex centred finite volume solver for Lagrangian solid dynamics, J. Comput. Phys. 300 (2015) 387–422.
[24] J. Bonet, A.J. Gil, C.H. Lee, M. Aguirre, R. Ortigosa, A first order hyperbolic framework for large strain computational solid dynamics. Part I : Total Lagrangian isothermal elasticity, Comput. Methods Appl. Mech. Engrg. 283 (2015) 689–732.
[25] A.J. Gil, C.H. Lee, J. Bonet, R. Ortigosa, A first order hyperbolic framework for large strain computational solid dynamics. Part II : Total Lagrangian compressible, nearly incompressible and truly incompressible elasticity, Comput. Methods Appl. Mech. Engrg. 300 (2016) 146–181.
[26] O.I. Hassan, A. Ghavamian, C.H. Lee, A.J. Gil, J. Bonet, F. Auricchio, An upwind vertex centred finite volume algorithm for nearly and truly incompressible explicit fast solid dynamic applications: Total and Updated Lagrangian formulations, J. Comput. Phys. : X 3 (2019) 100025.
[27] G. Scovazzi, B. Carnes, X. Zeng, S. Rossi, A simple, stable, and accurate linear tetrahedral finite element for transient, nearly, and fully incompressible solid dynamics: a dynamic variational multiscale approach, Int. J. Numer. Methods Eng. 106 (2016) 799–839.
[28] S. Rossi, N. Abboud, G. Scovazzi, Implicit finite incompressible elastodynamics with linear finite elements: A stabilized method in rate form, Comput. Methods Appl. Mech. Engrg. 311 (2016) 208–249.
[29] C. Sansour, On the physical assumptions underlying the volumetric-isochoric split and the case of anisotropy, Eur. J. Mech. A Solids 27 (2008) 28–39.
[30] J. Bonet, R.D. Wood, Nonlinear Continuum Mechanics for Finite Element Analysis, Cambridge University Press, 1997.
[31] C.O. Horgan, J.G. Murphy, On the volumetric part of strain-energy functions used in the constitutive modeling of slightly compressible solid rubbers, Int. J. Solids Struct. 46 (2009) 3028–3085.
[32] J.C. Simo, R.L. Taylor, K.S. Pister, Variational and projection methods for the volume constraint in finite deformation elasto-plasticity, Comput. Methods Appl. Mech. Engrg. 51 (1–3) (1985) 177–208.
[33] C. Miehe, Aspects of the formulation and finite element implementation of large strain isotropic elasticity, Internat. J. Numer. Methods Engrg. 12 (1994) 1981–2004.
[34] C.H. Liu, G. Hofstetter, H.A. Mang, 3D finite element analysis of rubber-like materials at finite strains, Eng. Comput. 11 (2) (1994) 111–128.
[35] R. Codina, S. Badia, J. Baiges, J. Principe, Variational multiscale methods in computational fluid dynamics, in: R.d.B. E. Stein, T. Hughes (Eds.), Encyclopedia of Computational Mechanics, John Wiley & Sons Ltd., 2017, pp. 1–28.
[36] S. Badia, R. Codina, Unified stabilized finite element formulations for the Stokes and the Darcy problems, SIAM J. Numer. Anal. 47 (3) (2009) 1971–2000.
[37] R. Codina, Stabilization of incompressibility and convection through orthogonal sub-scales in finite element methods, Comput. Methods Appl. Mech. Engrg. 190 (2000) 1579–1599.
[38] H.A. Van der Vorst, Bi-CGSTAB: A fast and smoothly converging variant of Bi-CG for the solution of nonsymmetric linear systems, SIAM, J. Sci. Stat. Comput. 13 (2) (1992) 631–644.
[39] S. Balay, S. Abhyankar, M.F. Adams, J. Brown, P. Brune, K. Buschelman, L. Dalcin, V. Eijkhout, W.D. Gropp, D. Kaushik, M.G. Knepley, D.A. May, L. Curfman McInnes, R.T. Mills, T. Munson, K. Rupp, P. Sanan, B.F. Smith, S. Zampini, H. Zhang, H. Zhang, PETSc Web page, 2015, http://www.mcs.anl.gov/petsc.
[40] J. Chung, G.M. Hulbert, A Time Integration Algorithm for Structural Dynamics with improved numerical dissipation: The generalized-α method, J. Appl. Mech. 60 (2) (1993) 371–375.